CLM - R 18

United Kingdom Atomic Energy Authority

RESEARCH GROUP

Report

THE DESIGN, CONSTRUCTION, INSTRUMENTATION AND PERFORMANCE OF AN 8 x 2 INCH SHOCK TUBE

R. HIDE
N. H. PRICE
P. A. SHATFORD

Culham Laboratory,
Culham, Abingdon, Berkshire
1962

Available from H.M. Stationery Office
TEN SHILLINGS NET.

U.D.C.
533.6.011.72

UNCLASSIFIED
(Approved for Sale)

CLM - R 18

THE DESIGN, CONSTRUCTION, INSTRUMENTATION AND PERFORMANCE OF THE A.E.R.E. 8" x 2" SHOCK TUBE

By

R. Hide, N.H. Price, P.A. Shatford.

ABSTRACT

The theory of gas flow in a shock tube is outlined and augmented by tables of useful numerical data on shocks. Details are given of the special design considerations necessary in the construction of a large shock tube. Instrumentation is discussed in three parts dealing respectively, with the filling of the tube with gases A and B to the desired pressures, the detection of the shock and the timing of its speed by electronic techniques, and an optical system used for making 'Toepler-Schlieren' and 'shadowgraph' observations of the gas flow associated with the shock. Finally a series of calibration experiments is described.

U.K.A.E.A. Research Group,
Culham Laboratory,
Nr. Abingdon,
Berks.

May, 1962

CONTENTS

LIST OF PLATES

LIST OF FIGURES

LIST OF FIGURES

(continued)

LIST OF TABLES

1. INTRODUCTION

1. In 1955 the Shock Wave Group was established at A.E.R.E., Harwell to carry out in shock tubes fundamental studies of magnetohydrodynamics, of the physical properties of hot gases, of shock diffraction and of the structure of shock waves[1].

2. A shock tube consists essentially of a long tube separated into two compartments by means of a diaphragm. These compartments are usually termed the 'compression' and 'expansion' chambers. In normal operation they are filled with suitable gases to the desired pressures p_4 and p_1, the compression chamber containing the higher pressure gas (see Fig. 1.1). On rupturing the diaphragm, the gas at the high pressure (A) expands into the expansion chamber and thus compresses gas B. This compression wave rapidly builds up into a shock which propagates through the gas B, raising its temperature and accelerating it into motion along the tube.

3. A convenient measure of the strength of a shock wave is its speed relative to the unshocked gas ahead of it, divided by the speed of sound. This is the 'shock Mach number', M, which is directly related to the conditions behind the shock (see Para.18). When $(p_4 - p_1)/p_1$ tends to zero, we have the 'acoustic limit' of a weak shock wave, for which M = 1. When $(p_4 - p_1)/p_1$ tends to infinity, M tends to a finite limit depending on the ratio of the initial temperatures of gases A and B and also of their gramme molecular weights. (See equation 1.14.)

4. Several shock tubes were built by the Shock Wave Group and a variety of scientific investigations carried out[2][3][4][5][6][13][14][15]. The purpose of the largest of these shock tubes, some 40 feet long and having a rectangular working section of 8" x 2", was the study of relaxation effects in gases, of shock diffraction and of shock structure. Because impurities have to be avoided when studying relaxation effects, the expansion chamber was constructed as a vacuum vessel, capable of being evacuated to a pressure of 2×10^{-5}mm Hg, before being filled with gas B.

5. There are practical limitations on the maximum value of M attainable in a shock tube. Having chosen the most favourable combination of gases, A and B, (see equation 1.14) the strongest shocks are produced at the highest practical value of p_4, determined by the strength of the compression chamber and the lowest practical value of p_1, determined by the onset of molecular rather than hydrodynamic flow, which arises when the collisional mean free path in gas B becomes comparable with the linear dimensions of the shock tube. The 8" x 2" shock tube was designed to produce shocks of strength up to about 14, so that crucial experiments on shock structure, involving the study of shocks of $M \geq 5$, could be carried out.

6. A novel feature of the design, incorporated for ease of construction, must be mentioned here. Although the working cross section of the shock tube is rectangular, dimensions 8" x 2", the cross section of the first 20' of the tube (total length 40') is circular, internal diameter 12". The connection between the circular and rectangular parts of the tube is made via a short length (5') of the tube of rectangular cross section, varying from 8" x 8" at the end where it meets the 'circular section' to 8" x 2" where it merges into the 'working section'. One incidental effect of this converging section is a slight but nevertheless significant amplification of the shock strength as it passes from one end to the other.

7. The shock tube came into operation in the summer of 1957. Having calibrated it and tested its general performance, two experiments were carried

out. The first, part of a proposed programme on shock diffraction, was an investigation on the motion of shocks in a curved channel[6]. In the second experiment a study of the structure of strong shocks in argon was initiated. However, at the end of 1957 the A.E.R.E. Shock Wave Group closed down for a variety of non-technical reasons and the 8" x 2" shock tube was moved to the Department of Fluid Dynamics of Manchester University, where it is now being used for the study of relaxation effects in gases.

8. Although there are in existence in various places a number of large shock tubes, special design considerations were necessary in the construction of a shock tube to meet our requirements. The experience thus gained has been novel and is recorded in this report because it could be of value to other workers.

9. The report is made up as follows. The theory of flow in a shock tube is outlined in para 10 et seq, where useful numerical data on shocks are given in a series of tables. Section 2 is an account of the general lay-out of the apparatus and Section 3 deals with the details of the design and construction of the compression and expansion chambers, together with the pumping system. Instrumentation is discussed in Section 4, which is divided into three parts dealing, respectively, with the filling of the tube with gases A and B to the desired pressures, the detection of the shock and the timing of its speed by means of high speed electronic techniques, and an optical system used for making 'Toepler-Schlieren' and 'shadowgraph' observations of the gas flow associated with the shock. Finally, in Section 5, a series of calibration experiments is described.

The initial phase of the flow in a shock tube of uniform bore

10. The history of the application of the shock tube has been sketched by Bitondo and Lobb[9] and several treatments of the theory of the initial phase of the flow arising on bursting the diaphragm have been published (see e.g. Lukasiewicz[10]). In order to establish the notation, we shall consider briefly the initial phase of the flow, assuming first that the expansion chamber has a uniform bore, and then introducing a correction for the effect of the converging section.

11. This is illustrated by Fig.1.1. Before $t = 0$, at which time the diaphragm is ruptured, the compression chamber, of length x_c is filled with gas A of molecular weight μ_4, ratio of principal specific heats γ_4, to a pressure p_4 and temperature T_4. The expansion chamber of length x_E is filled with gas B, molecular in weight μ_1, ratio of principal specific heats γ_1, to pressure p_1 and at temperature T_1.

12. On bursting the diaphragm, gas A expands out of the compression chamber, thus acquiring a velocity U_3 and pressure p_3, temperature T_3 and density ρ_3. Conditions (3) are non-uniform, that is to say, they vary from $U_3 = 0$ and $p_3 = p_4$ at the head of the rarefaction wave moving into gas A at the sound speed a_4, where

$$a^2 = RT/\mu \qquad (1.1)$$

(R being the universal gas constant) to $p_3 = p_2$ and $U_3 = U_2$ at the contact surface (see below, and Fig. 1.1.)

13. The gas A emerging from the compression chamber can be regarded as a piston compressing gas B. As a result of this compression, a shock wave is sent into gas B at U cm/sec., raising the pressure, density and temperature of this gas from p_1, ρ_1 and T_1 to p_2, ρ_2 and T_2 respectively, and accelerating the gas from rest relative to the tube, to a uniform velocity U_2, where $U_2 < U$ (see equation 1.4).

14. As time progresses the shock travels along the tube until it strikes the closed end. At this point, the gas molecules behind the incident shock are brought to rest. This results in a reflected shock, which raises the pressure density and temperature further, to p_5, ρ_5 and T_5.

15. The rarefaction wave continues to move into the compression chamber, thus expanding gas A which is thus accelerated along the tube towards the expansion chamber. On meeting the closed end of the compression chamber the rarefaction wave is reflected. This reflected wave accelerates as it progresses along the tube.

16. The length of the shock tube nas been discussed in detail by several authors[11][12]. A lower limit to the length of the expansion chamber, X_E, is determined by the tube cross section. Near the diaphragm section the gas flow is usually quite complicated, and it is only when the incident shock has progressed about several tube diameters downstream of the diaphragm section that transverse waves have disappeared and the shock is sensibly plane.

17. If the incident shock is to be studied, the length of the compression chamber X_c should be sufficiently large to ensure that the rarefaction wave reflected from the closed end of the compression chamber, and the shock wave reflected from the end of the expansion chamber interact with one another, and with the contact surface between gases A and B after the contact surface has passed the observation section, and not before.

18. In order to make detailed calculations it is necessary to relate the desired shock strength to the initial conditions. The theory of the plane shock wave, which is a straightforward application of equations of continuity, momentum and energy leading to relations between conditions on either side of a shock, was first given many years ago by Rankine and Hugoniot. If U is the speed of the shock front relative to the gas ahead of it, in which the pressure density and temperature are, respectively, p_1, ρ_1 and T_1, and p_2, ρ_2 and T_2 are the corresponding values of these parameters in the shocked gas, and U_2 is the velocity of this shocked gas relative to the unshocked gas ahead of the shock front, then

$$p_2/p_1 = \beta_1/\left[M^2\ (\beta_1 + 1) - 1\ \right] \tag{1.2}$$

$$U/(U-U_2) = \rho_2/\rho_1 = \beta_1/\left[1 + (\beta_1 - 1)/M^2\ \right] \tag{1.3}$$

$$\frac{T_2}{T_1} = \frac{p_2\rho_1}{p_1\rho_2} = \left(\frac{a_2}{a_1}\right)^2 = \frac{M^2}{\beta_1^2}\left[\beta_1 + 1 - 1/M^2\right] \tag{1.4}$$

$$U_2/a_1 = M(\beta_1 - 1)(1 - 1/M^2)/\beta_1 \tag{1.5}$$

where

$$\beta \equiv (\gamma + 1)/(\gamma - 1);\quad M \equiv U/a_1, \tag{1.6}$$

a being the speed of sound and γ the ratio between the principal specific heats. In writing these equations, M has been chosen as the independent variable simply because it is the quantity we were able to measure more or less directly. In their original discussion, Rankine and Hugoniot related pressure and density ratios, thus

$$\frac{p_2}{p_1} = \left[\beta_1\frac{\rho_2}{\rho_1} - 1\ \right] \Big/ \left[\beta_1 - \rho_2/\rho_1\right] \tag{1.7}$$

The entropy change per unit mass at the shock front,

$$S_2 - S_1 = C_v \left[\log e \frac{p_2}{p_1} - \gamma_1 \log \frac{\rho_2}{\rho_1} \right] \qquad (1.8)$$

where C_v is the specific heat at constant volume.

19. Denoting by subscript 5 the region behind the shock reflected from the end of the expansion chamber, if the shock front moves towards the compression chamber with speed U_R a further application of the Rankine-Hugoniot relation leads to the following expressions for the properties of the twice shocked gas:-

$$U_R = U \left[2 + (\beta_1 - 2)/M^2 \right] / \beta_1 \qquad (1.9)$$

$$p_5/p_2 = \left[M^2(2 + \beta_1) - 2 \right] / \left[M^2 + \beta_1 \right] \qquad (1.10)$$

$$\rho_5/\rho_2 = \left[M^2(\beta_1 + 1) - 1 \right] / \left[2M^2 + \beta_1 - 2 \right] \qquad (1.11)$$

$$\frac{T_5}{T_2} = \left[\frac{M^2(2 + \beta_1) - 2}{M^2(\beta_1 + 1) - 1} \right] \left[\frac{2M^2 + \beta_1 - 2}{M^2 + \beta_1 - 1} \right] \qquad (1.12)$$

Finally, by considering the expansion of the compression chamber gas from conditions 4 to 3 and applying the appropriate boundary conditions at the contact surface, namely $p_3 = p_2$, $U_3 = U_2$ a relation between the incident shock strength, M, and the starting conditions can be found, namely

$$\frac{p_4}{p_1} = \left[\left(\frac{\beta_1 + 1}{\beta_1} \right) M^2 - \frac{1}{\beta_1} \right] / \left[1 - \left(\frac{\beta_1 - 1}{\beta_1(\beta_4 - 1)} \right) \left(\frac{a_1}{a_4} \right) \left(M - \frac{1}{M} \right) \right]^{(\beta_4 + 1)} \qquad (1.13)$$

It is noteworthy that as p_4/p_1 tends to infinity M tends to a finite limit M* where if $(M^*)^2 \gg 1$, to a good accuracy.

$$M^* = \left(\frac{\beta_1(\beta_4 - 1)}{(\beta_1 - 1)} \right) \left(\frac{a_4}{a_1} \right) \qquad (1.14)$$

The physical reason for this limit is easy to appreciate. It is due to the fact that even on expanding gas A into a vacuum, the speed to which it is thus accelerated cannot exceed a value of the same order as the root-mean-square velocity associated with molecular thermal motion, the exact value being $a_4/[2/(\gamma_4 - 1)]^{\frac{1}{2}}$; the dependence of M* on a_4 is evident in the last equation.

20. Various simplifying assumptions are made in deducing equations 1.2 to 1.8. These are, that

(a) the diaphragm is removed 'instantaneously' and the flow can be treated as one-dimensional;

(b) viscous friction between the fluid and the shock tube wall can be ignored;

(c) heat losses due to conduction at the wall can be ignored;

(d) the specific heat of the gas is independent of temperature, which is equivalent to ignoring thermal dissociation, excitation and ionization.

There is experimental evidence that (b) and (c) are valid except at the lowest pressures, and (d) is valid except for very strong shocks (see reference 4).

21. As regards assumption (a), although the flow near the diaphragm section is quite complicated, by the time the shock has progressed a distance along the tube equal to several tube diameters - the exact value depending on, and increasing with, M -, provided the tube bore is uniform transverse disturbances have negligible amplitude, and if no substantial deviations from assumptions (b) and (c) arise, the shock is plane and the flow associated with it one-dimensional (see reference 12).

22. We conclude this section with tables of useful numerical data based on equations 1.2 to 1.8, which are not readily available elsewhere. Some of these calculations were carried out by Mr. M.E. English, using the University of Durham Pegasus Computer, and we are grateful to him for permission to present them here.

TABLE 1.1

MOLECULAR WEIGHT (μ) AND RATIO OF PRINCIPAL SPECIFIC HEATS (γ) OF VARIOUS GASES

GAS	H_2	He	Ne	N_2	Air	$C_2 H_6$
γ	1.40	1.63	1.64	1.41	1.40	1.22
μ	2.02	4.00	20.18	28.02	29.95	30.07

GAS	K	A	CS_2	Kr	Xe	Cs
γ	1.67	1.67	1.24	1.69	1.67	1.67
μ	39.10	39.94	76.14	83.80	131.30	132.91

TABLE 1.2

THE LIMITING SHOCK STRENGTH, M^*, CORRESPONDING TO $P_4/P_1 \to \infty$ FOR DIFFERENT GAS COMBINATIONS WHEN THE SYSTEM IS INITIALLY ISOTHERMAL ($T_4 = T_1$).

(REAL GAS EFFECTS IGNORED)

GAS A	Air	H_2	He	He	He	He	He	He	He	He	H_2	H_2	H_2	H_2	He	He	H_2	H_2	H_2	H_2	H_2	H_2
GAS B	Air	He	Ne	N_2	Air	C_2H_6	K	A	CS_2	Kr	Ne	N_2	Air	C_2H_6	Xe	Cs	K	A	CS_2	Kr	Xe	Cs
M^*	6.16	8.69	9.49	11.0	11.2	11.3	13.2	13.3	17.8	19.3	19.3	22.4	22.8	23.0	24.0	24.2	26.9	27.2	36.6	39.5	49.3	49.6

TABLE 1.3

TABLE OF P_4/P_1 RATIO REQUIRED TO PRODUCE SHOCK OF STRENGTH M FOR DIFFERENT GAS COMBINATIONS WHEN SYSTEM IS INITIALLY ISOTHERMAL ($T_4 = T_1$), 'REAL GAS' EFFECTS BEING IGNORED

GAS A	AIR	H_2	He	He	He	He	He	He	He	He	H_2	GAS A
GAS B	AIR	He	Ne	N_2	Air	C_2H_6	K	A	CS_2	Kr	Ne	GAS B
SHOCK STRENGTH M												SHOCK STRENGTH M
2	3.34 1	1.81 1	1.16 1	9.71 0	9.57 0	9.06 0	8.92 0	8.86 0	6.82 0	7.27 0	8.34 0	2
3	6.33 2	1.48 2	6.17 1	4.44 1	4.31 1	4.02 1	3.58 1	3.53 1	2.29 1	2.40 1	3.10 1	3
4	1.78 4	1.10 3	2.75 2	1.65 2	1.58 2	1.45 2	1.13 2	1.11 2	6.00 1	6.11 1	8.93 1	4
5		9.60 3	1.26 3	5.89 2	5.52 2	5.01 2	3.30 2	3.20 2	1.40 2	1.38 2	2.29 2	5
6	M* = 6.16	1.30 5	6.80 3	2.23 3	2.03 3	1.81 3	9.48 2	9.07 2	3.11 2	2.93 2	5.55 2	6
7			5.39 4	9.79 3	8.53 3	7.41 3	2.84 3	2.67 3	6.73 2	6.04 2	1.32 3	7
8		M* = 8.69		5.77 4	4.68 4	3.90 4	9.33 3	8.60 3	1.46 3	1.23 3	3.13 3	8
9			M* = 9.49		4.31 5	3.32 5	3.62 4	3.23 4	3.23 3	2.54 3	7.61 3	9
10				M* = 11.0			1.86 5	1.57 5	7.44 3	5.35 3	1.93 4	10
11					M* = 11.2	M* = 11.3	1.61 6	1.23 6	1.83 4	1.17 4	5.18 4	11
12									4.94 4	2.73 4	1.51 5	12
13							M* = 13.2	M* = 13.3	1.54 5	6.93 4	4.97 5	13
14									5.91 5	1.99 5	1.93 6	14
15									3.23 6	6.82 5	9.51 6	15
16										3.12 6	6.82 7	16
17									M* = 17.8	2.37 7	9.43 8	17
18												18
19										M* = 19.3	M* = 19.3	19
20												20
21												21
22												22
23												23
24												24
25												25

(The second figure gives the power of 10 by which the first figure has to be multiplied)

TABLE 1.3 (Continued)

GAS A	H_2	H_2	H_2	He	He	H_2	H_2	H_2	H_2	H_2	H_2	GAS A
GAS B	N_2	Air	C_2H_6	Xe	Cs	K	A	CS_2	Kr	Xe	Cs	GAS B
SHOCK STRENGTH M												SHOCK STRENGTH M
2	7.33 0	7.26 0	6.90 0	6.64 0	6.62 0	7 10 0	7.07 0	5.80 0	6.26 0	5.90 0	5.89 0	2
3	2.52 1	2.48 1	2.33 1	2.03 1	2.02 1	2.29 1	2.27 1	1.68 1	1.81 1	1.63 1	1.62 1	3
4	6.71 1	6.54 1	6.10 1	4.76 1	4.74 1	5.66 1	5.59 1	3.76 1	4.00 1	3.44 1	3.43 1	4
5	1.58 2	1.53 2	1.42 2	9.85 1	9.77 1	1.23 2	1.21 1	7.39 1	7.73 1	6.36 1	6.33 1	5
6	3.48 2	3.34 2	3.08 2	1.89 2	1.87 2	2.48 2	2.43 2	1.34 2	1.38 2	1.08 2	1.08 2	6
7	7.42 2	7.05 2	6.46 2	3.49 2	3.44 2	4.79 2	4.67 2	2.32 2	2.34 2	1.74 2	1.73 2	7
8	1.56 3	1.47 3	1.33 3	6.26 2	6.16 2	9.03 2	8.76 2	3.87 2	3.81 2	2.70 2	2.68 2	8
9	3.28 3	3.05 3	2.75 3	1.11 3	1.09 3	1.68 3	1.62 3	6.31 3	6.07 2	4.07 2	4.03 2	9
10	7.00 3	6.41 3	5.73 3	1.96 3	1.92 3	3.11 3	2.98 3	1.01 3	9.49 2	6.00 2	5.94 2	10
11	1.53 4	1.38 4	1.22 4	3.49 3	3.40 3	5.77 3	5.49 3	1.60 3	1.47 3	8.71 2	8.61 2	11
12	3.47 4	3.06 4	2.68 4	6.28 3	6.09 3	1.08 4	1.02 4	2.53 3	2.24 3	1.25 3	1.23 3	12
13	8.28 4	7.12 4	6.14 4	1.16 4	1.12 4	2.07 4	1.94 4	3.97 3	3.42 3	1.78 3	1.75 3	13
14	2.11 5	1.76 5	1.49 5	2.20 4	2.10 4	4.05 4	3.75 4	6.25 3	5.20 3	2.51 3	2.47 3	14
15	5.90 5	4.74 5	3.92 5	4.35 4	4.13 4	8.19 4	7.47 4	9.86 3	7.91 3	3.52 3	3.46 3	15
16	1.86 6	1.42 6	1.14 6	9.09 4	8.55 4	1.72 5	1.55 5	1.57 4	1.21 4	4.93 3	4.83 3	16
17	6.89 6	4.92 6	3.80 6	2.04 5	1.90 5	3.81 5	3.36 5	2.51 4	1.85 4	6.90 3	6.75 3	17
18	3.24 7	2.10 7	1.54 7	5.07 5	4.63 5	8.99 5	7.76 5	4.06 4	2.86 4	9.64 3	9.41 3	18
19	2.19 8	1.22 8	8.22 7	1.45 6	1.29 6	2.30 6	1.93 6	6.67 4	4.45 4	1.35 4	1.31 4	19
20	2.77 9	1.18 9	6.90 8	5.05 6	4.33 6	6.56 6	5.32 6	1.12 5	7.00 4	1.89 4	1.84 4	20
21				2.44 7	1.97 7	2.16 7	1.67 7	1.90 5	1.12 5	2.66 4	2.58 4	21
22	M* = 22.4	M* = 22.8	M* = 23.0	2.12 8	1.53 8	8.64 7	6.26 7	3.33 5	1.81 5	3.76 4	3.63 4	22
23						4.63 8	3.04 8	5.98 5	3.00 5	5.34 4	5.14 4	23
24				M* = 36.6	M* = 24.2	3.95 9	2.21 9	1.11 6	5.06 5	7.62 4	7.32 4	24
25							3.26 10	2.16 6	8.78 5	1.10 5	1.05 5	25
						M* = 26.9						
							M* = 27.2	M* = 36.6	M* = 39.5	M* = 49.3	M* = 49.6	

(The second figure gives the power of 10 by which the first figure has to be multiplied)

The converging section

23. We must now consider the effect on the shock of the presence of a converging channel in which the area is gradually reduced by a factor of 4 (from 8" x 8" to 8" x 2", see Fig. 3.2). The theory of the passage of a shock along such a channel has been discussed by Chester[16], Witham[17] and Hide[15]. Again, viscous friction ahd heat conduction at the walls are ignored. Hide, for example, has given an equation relating the strength M_o of the shock as it emerges from the channel to the strength M_i of the incident shock, in terms of the cross sectional areas of the two ends of the channel, A_i and A_o respectively, namely:

$$M_o/M_i = \left[M_i^{-2} + (1 - M_i^{-2})(A_i/A_o)^k\right]^{\frac{1}{2}} \qquad (1.15)$$

where K is a slowly varying function of M_i if γ_1 is not too close to unity. Table 1.4, taken from Whitham's paper, illustrates the variation of K with M_i for two values of γ_1 namely 1.4 and 1.67, and Table 1.5 illustrates the dependence on γ_1 within the range 1.4 to 1.67 of the value to which K tends asymptotically as M_i tends to infinity.

24. In Table 1.6 values of M_o/M_i for $\gamma_1 = 1.67$ and $\gamma_1 = 1.4$ are listed for the case under consideration, namely, $A_o/A_i = 0.25$, for different values of M_i, and with the aid of this table, it is possible to calculate the enhancement factor to be expected. That this amplification was achieved in practice is borne out by the results given below in Section 5.

TABLE 1.4

M_i	1	1.2	1.4	1.5	1.7	2.0	3.0	5.0	∞
$K(\gamma_1 = 1.4)$	0.500	0.470	0.460	0.450	0.440	0.430	0.410	0.400	0.394
$K(\gamma_1 = 1.67)$	0.500	0.485	0.480	0.475	0.470	0.465	0.455	0.455	0.451

TABLE 1.5

γ_1	1.4	1.45	1.5	1.55	1.6	1.65	1.67
$K(M_i = \infty)$	0.394	0.407	0.418	0.427	0.439	0.447	0.451

TABLE 1.6

M_i	$\gamma_1 = 1.4$		$\gamma_1 = 1.67$		M_i	$\gamma_1 = 1.4$		$\gamma_1 = 1.67$	
	M_o	M_o/M_i	M_o	M_o/M_i		M_o	M_o/M_i	M_o	M_o/M_i
1.000	1.000	1.000	1.000	1.000	4.000	5.224	1.306	5.400	1.350
1.200	1.366	1.114	1.363	1.138	5.000	6.503	1.306	6.790	1.358
1.400	1.674	1.198	1.685	1.206	6.000	7.878	1.312	8.166	1.361
1.500	1.820	1.215	1.848	1.232	7.000	9.184	1.312	9.562	1.366
1.700	2.120	1.246	2.135	1.254	8.000	10.496	1.312	10.928	1.366
2.000	2.544	2.272	2.592	1.296	9.000	11.808	1.313	12.294	1.366
2.500	3.220	1.289	3.310	1.324	10.000	13.120	1.312	13.660	1.366
3.000	3.891	1.297	4.005	1.335	∞	∞	1.314	∞	1.367

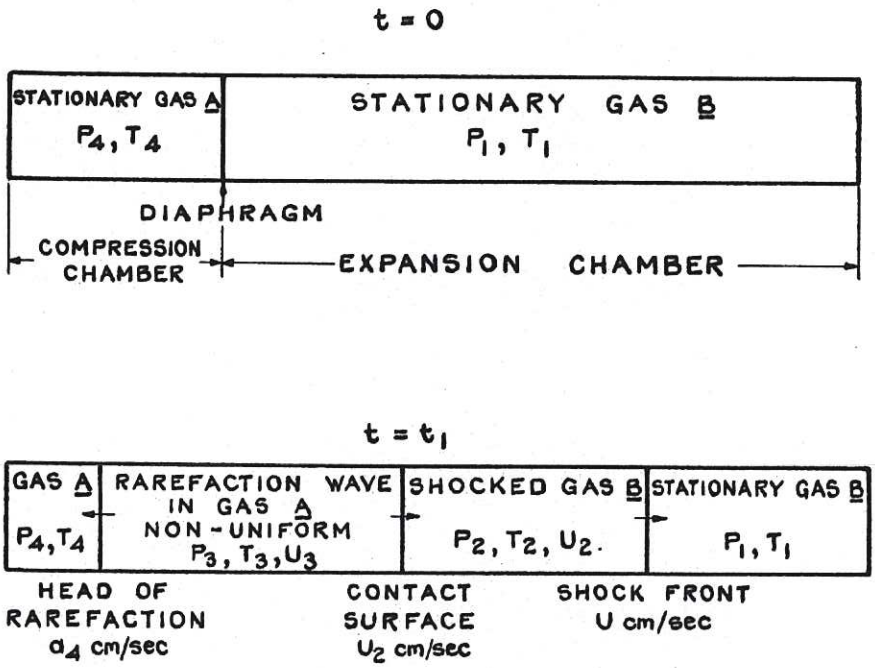

CLM-R18 FIG. 1·1. ILLUSTRATING THE INITIAL PHASE OF THE FLOW IN A SHOCK TUBE FOLLOWING THE BURSTING OF THE DIAPHRAGM.

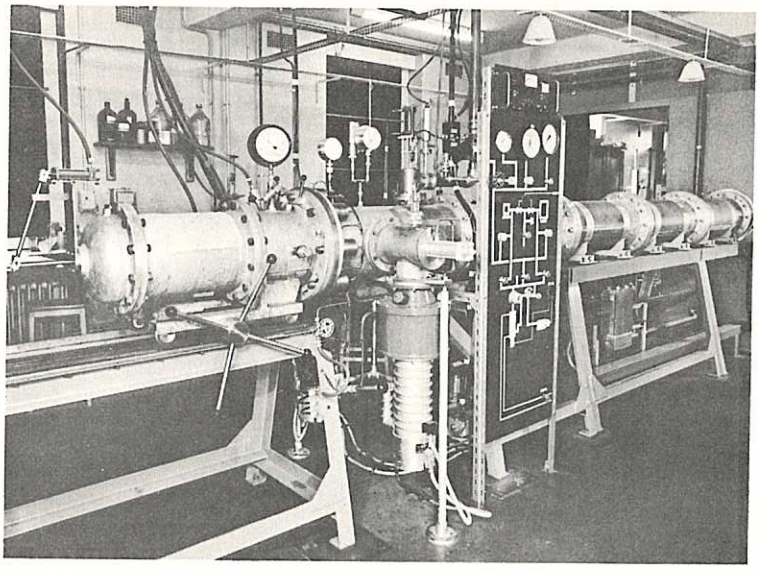

ILLUSTRATING GENERAL LAYOUT OF SHOCK TUBE

Plate 2.1. This shows the operating room, looking along the shock tube from the compression chamber end (see Fig. 2.1).

From left to right are the hydraulically operated plunger for bursting the diaphragm, compression chamber, diaphragm flange, full view of one of the 6" bore diffusion pumps, the gas decanting panel and the last three sections of the first part of the expansion chamber. The compression chamber is mounted on a wheeled trolley moving on rails to facilitate the withdrawal of the chamber in order to change the diaphragm.

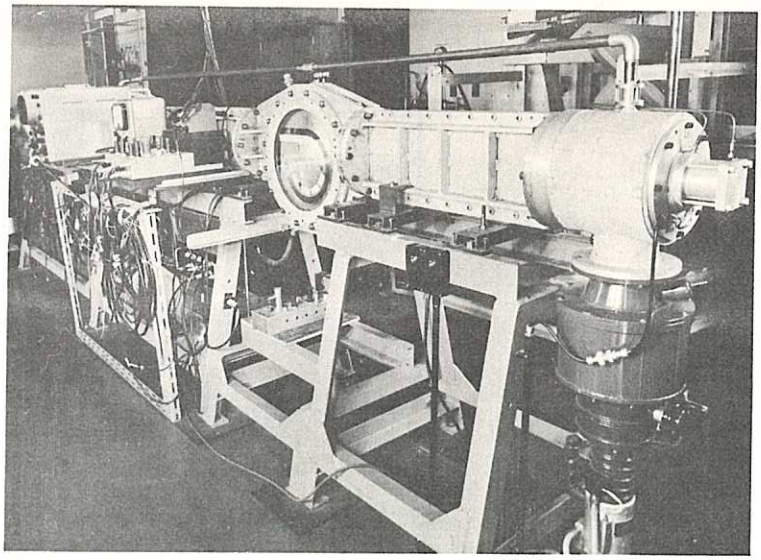

ILLUSTRATING GENERAL LAYOUT OF SHOCK TUBE

Plate 2.2. This shows the observation room (see Fig. 2.1) looking along the shock tube from the other end. From right to left are the 4" diffusion pump, part 5 of the expansion chamber, the diffraction chamber with a model in position. Parts 2 and 3 of the expansion chamber are obscured by two of the 'gold film' amplifiers, a valve voltmeter and an oscilloscope. The copper tubing running above the shock tube is a pumping line.

2. GENERAL LAYOUT OF APPARATUS

25. The layout of the apparatus is shown in Fig. 2.1, which is a plan view of the whole laboratory. This laboratory consists of a large room divided into two compartments (operating room and observation room) by means of a light proof partition. (When photographic observations were made the observation room was completely blacked out to exclude extraneous light.)

26. The apparatus consists essentially of:

(a) The shock tube, down the middle of the laboratory (see Fig.2.1), the glass sided 'diffraction chamber' being required for Toepler-Schlieren and shadowgraph observations of the interaction of shocks with rigid surfaces (see above, para.8 et seq.and below, para.71 et seq).

(b) The shock detection system, the detector units being in the observation room and the associated electronics (timing units, delay units) in the operating room.

(c) The control system for remote operation of priming and firing units in the operating room.

(d) The Toepler-Schlieren and shadowgraph optical system, in the observation room.

Plates 2.1 and 2.2 are general views of the completed shock tube.

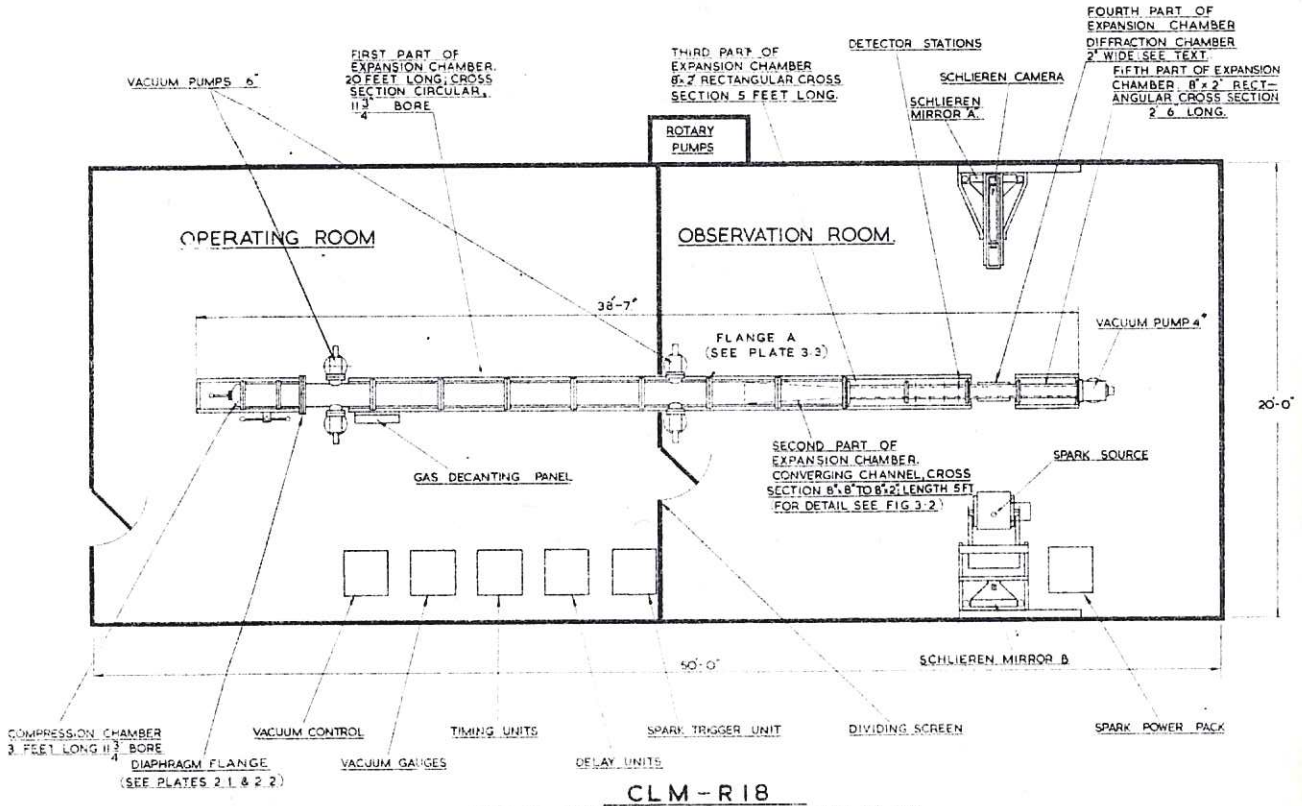

CLM-R18

FIG.2.1. SHOCK TUBE LAYOUT PLAN.

3. DESIGN AND CONSTRUCTION OF SHOCK TUBE

The Compression Chamber

27. This chamber (see Fig.2.1) was constructed to withstand, without leakage, pressures ranging from 0.1 to 10^4 torr (1 torr ≡ 1 mm Hg). Thus, when a gas A was not air (see Fig.1.1), it was possible to maintain a high level of purity, always better than 99 per cent, and generally much better than this value. This was achieved by using 'O' ring gaskets for all flanges and couplings.

28. The chamber is a steel cylinder, 3' long, 12" bore, having a hemispherical end, and coupled to the expansion chamber at the diaphragm clamping flange; details are given in Figs. 2.1 and 3.1, Plates 2.1 and 3.1.

Hydraulic Clamping Mechanism

29. The clamping mechanism (see Fig. 3.1 and Plates 3.1 and 3.2) was used to hold the compression and expansion chambers together. The mating flanges were each fitted with 'O' rings and the diaphragm was held between them. To ensure that the 'O' rings remained in position whenever the diaphragm flanges were separated each 'O' ring groove was of trapezoidal cross section. In this form of groove the 'O' ring is gently nipped and will not fall out. In an early design, pressure differences across the 'O' ring tended to force it into the bottom of its groove, thus causing leaks. This was remedied by drilling holes in the flange and thus connecting the underside of the groove to the compression chamber so equalising the pressure on both sides of the 'O' ring.

30. The eight hydraulic cylinders were fed with oil under pressure from a hand pump mounted on the tube frame. To release the locking ring the pistons were pumped out after operating a two way change-over valve in the oil supply. The locking ring could then be turned to allow the clamp nuts to pass through the release slots, and the compression chamber to be withdrawn.

31. The diaphragm material was 'Melinex' between 10^{-3} and 5×10^{-3} inches thick. ('Melinex'('Mylar' in the U.S.A.) is a terylene based transparent plastic material which is strong, elastic and very hard to tear.) Each diaphragm was prepared by cutting around a special template.

Expansion Chamber; Circular Part

32. The circular part of the expansion chamber (see Plates 2.1 and 3.2) was built up from flanged tubes, each 3' long and $11\frac{3}{4}$" bore. These tubes were fabricated from 1" thick aluminium plate, rolled to form 'U' sections which were then welded together to form tubes. The flanges were welded on and their respective faces machined flat and parallel to one another.

33. The maximum length which could be bored on the machines available was 4', so the tubes were machined in pairs, the bore register being transferred from pair to pair throughout the length of the complete circular section. On final assembly any small irregularities in the bore at the joints were removed by lapping with emery cloth. 'O' ring seals were fitted at each flanged joint of the expansion chamber.

The Converging Channel

34. The position of this part of the apparatus is illustrated in Fig. 2.1, the detailed construction is shown in Fig. 3.2, and a pictorial view is given in Plate 3.3.

35. The converging channel was constructed out of thick steel plates, with butt joints screwed together. The edges of the square mouth at the upstream end were bevelled down to a sharp edge to minimize their disturbing effect on the gas flow, and the corners were machined to be a close fit in the bore of the tube (see Plate 3.3).

Expansion Chamber, Rectangular Part

36. Figure 3.3 shows a section through this part of the tube. The steel bars, of square section, which formed the roof and floor carried straight grooves in which circular section rubber cord was fitted. The side plates, which were stiffened by welded heavy steel webs, were bolted to the roof and floor bars. The end flanges were welded to the side plates. Each coupling flange consisted, therefore, of four parts, namely, the two segments attached to the side walls and the ends of the floor and roof bars. One flange of each pair carried an 'O' ring groove of such a diameter as to intercept the longitudinal cord grooves so that the cord ends abutted against the 'O' rings and formed a vacuum seal.

Diffraction Chamber

37. A view of this component (see Section 2) is shown in Plate 3.4. The construction is similar to that of the rectangular sections, the steel side frames being bolted to shaped steel blocks to form a circular box. Circular rubber cord was again used for vacuum sealing.

38. The windows were of $1\frac{1}{2}$" thick Schlieren quality glass, optically finished. They were set in carefully machined circular steel frames with 'Hermetal' epoxy resin putty.

39. The two steel bars used to continue the 8" x 2" channel through the chamber were removable, together with their brackets, to leave a circular chamber. The centre of this chamber was 2" below the horizontal axis of the channel, this asymmetry providing more space below the channel to accommodate such models as those used in curved channel experiments[6].

The Vacuum System

40. For reasons given in section 1, the expansion chamber was constructed as a vacuum vessel capable of being evacuated to a pressure of 0.02 m.torr (2×10^{-5} mm Hg). The leak rate was such that on turning off the pumps the pressure rose at about 1 micro torr per second. Since the experimental procedure required a period of not more than 3 minutes between filling the expansion chamber with gas B and firing the shock tube, the degree of impurity due to leakage was only $2\frac{1}{2}$ per cent even at the lowest values of p_1 used, namely, 5 mtorr.

41. A schematic diagram of the pumping system is shown in Fig. 3.4. Four 6" diffusion pumps (Nos. 1 - 4) were arranged in diametrically opposed pairs at each end of the circular part of the expansion chamber and the fifth, a 4" pump, at the extreme end of the rectangular part of the tube. Each pump carried a liquid air trap and was coupled to the tube via specially designed valves, described in more detail below in para. 46 et seq. Preliminary pumping to reduce the pressure to 0.15 torr was achieved by means of one 450 litre/min. rotary pump (designated 'No.I' in Fig. 3.4). At this stage, the compression chamber was isolated from the pumps and the diffusion pumps were brought in to reduce further the pressure in the expansion chamber.

42. All the expansion chamber pressure gauges were mounted on a manifold which could be isolated from the rest of the system by pneumatic piston valves B-3

and B-4. B-3 was a normal sliding plate valve. B-4 was of special design (see below, para.46) similar to those fitted to the six inch pumps. It was used to isolate the pressure gauges prior to bursting the diaphragm, thus protecting these gauges from the pressure rise accompanying this event.

43. Although No.1 rotary pump was used for 'backing' the diffusion pumps during normal operation of the shock tube, it was convenient during extended periods of 'degassing' at pressures under 0.1 m.torr to use a somewhat smaller rotary pump (No.2, see Fig. 3.4) for this purpose.

44. All valves were operated remotely, either magnetically or pneumatically, and the complete system was interlocked to protect the equipment from damage which errors in procedure and power failures would otherwise have caused.

45. Low pressures in the range 0.02 to 100 m.torr were measured with Pirani and ionisation gauges. p_1 was determined by a 'shared volume' method described in Section 4. The accuracy in this measurement amounted to 0.1 per cent when p_1 was 1 torr.

Special Vacuum Valves

46. To avoid irregularities in the bore of the expansion chamber and yet to provide the large diameter ports required for rapid pumping at low pressures, special vacuum valves were developed (Fig. 3.5). When open, each valve seat projected into the bore of the tube. The seat was shaped to conform to the circular wall when in the closed position and by using an 'O' ring piston seal it was possible to provide a definite mechanical stop. Consequently, there was no danger of further seat movement as a result of the pressure rise associated with the passing shock wave. Rotation of the seat was prevented by guide rods.

47. Further piston seals were used to seal each valve into the ports in the tube wall. Each valve was fitted into the tube with suitable shims between the flange faces to obtain good alignment between the valve face and the tube bore.

48. The space between the two shaft sealing 'O' rings is vented to atmosphere to prevent undesirable high pressures building up between the rings in the event of a leak arising from the high pressure air cylinder.

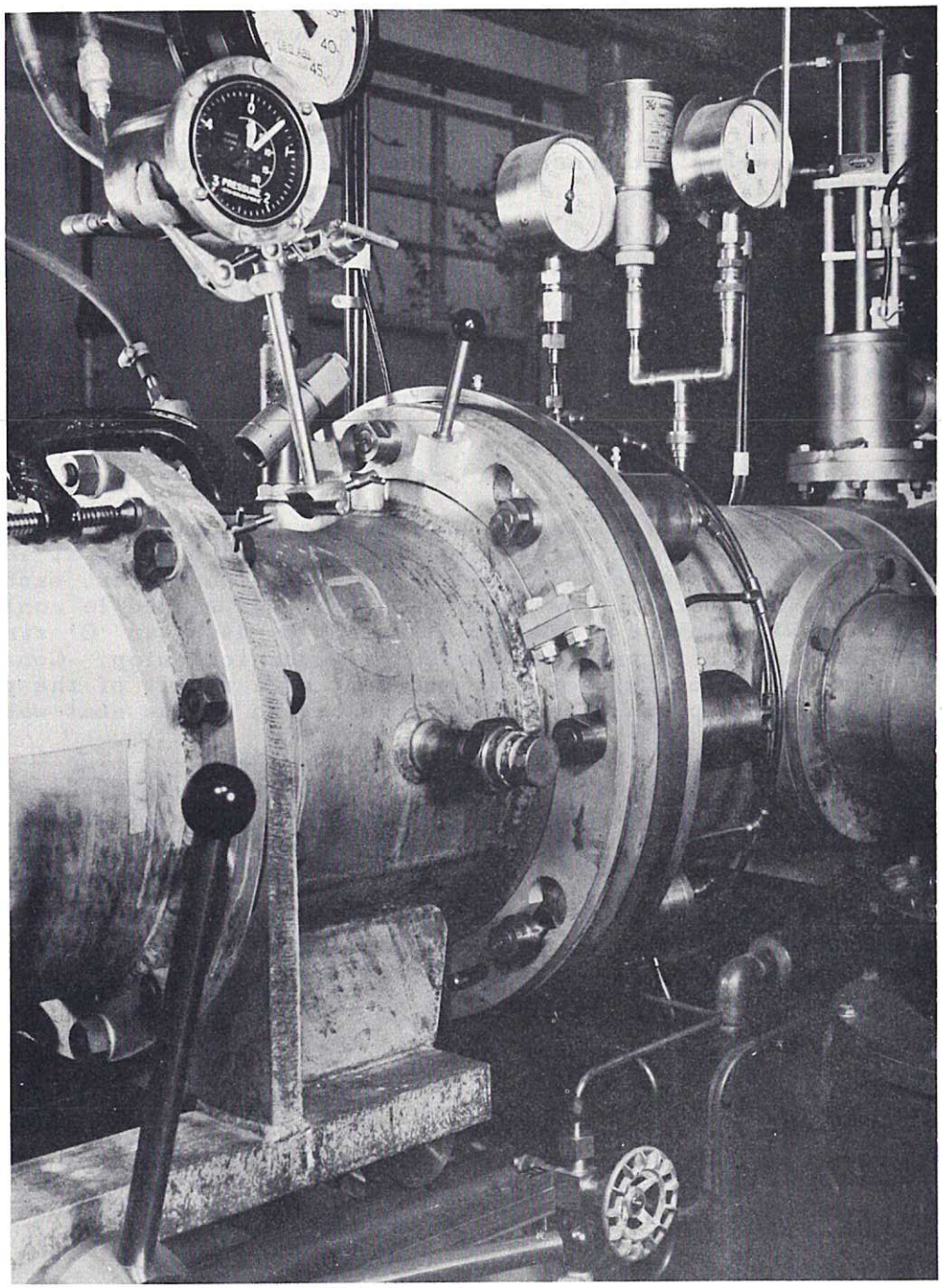

DIAPHRAGM FLANGE AND HYDRAULIC CLAMP

Plate 3.1. This picture illustrates the hydraulic clamping arrangement of the diaphragm flange where the compression chamber meets the expansion chamber. (The flange to the extreme left is the joint between two parts of the compression chamber.) The clamp is shown locked, the bayonet ring being in the closed position and the pressure in the 8 hydraulic cylinders (three of which can be seen) being 1600 p.s.i. (see pressure gauge, top centre). (See also Fig. 3.1).

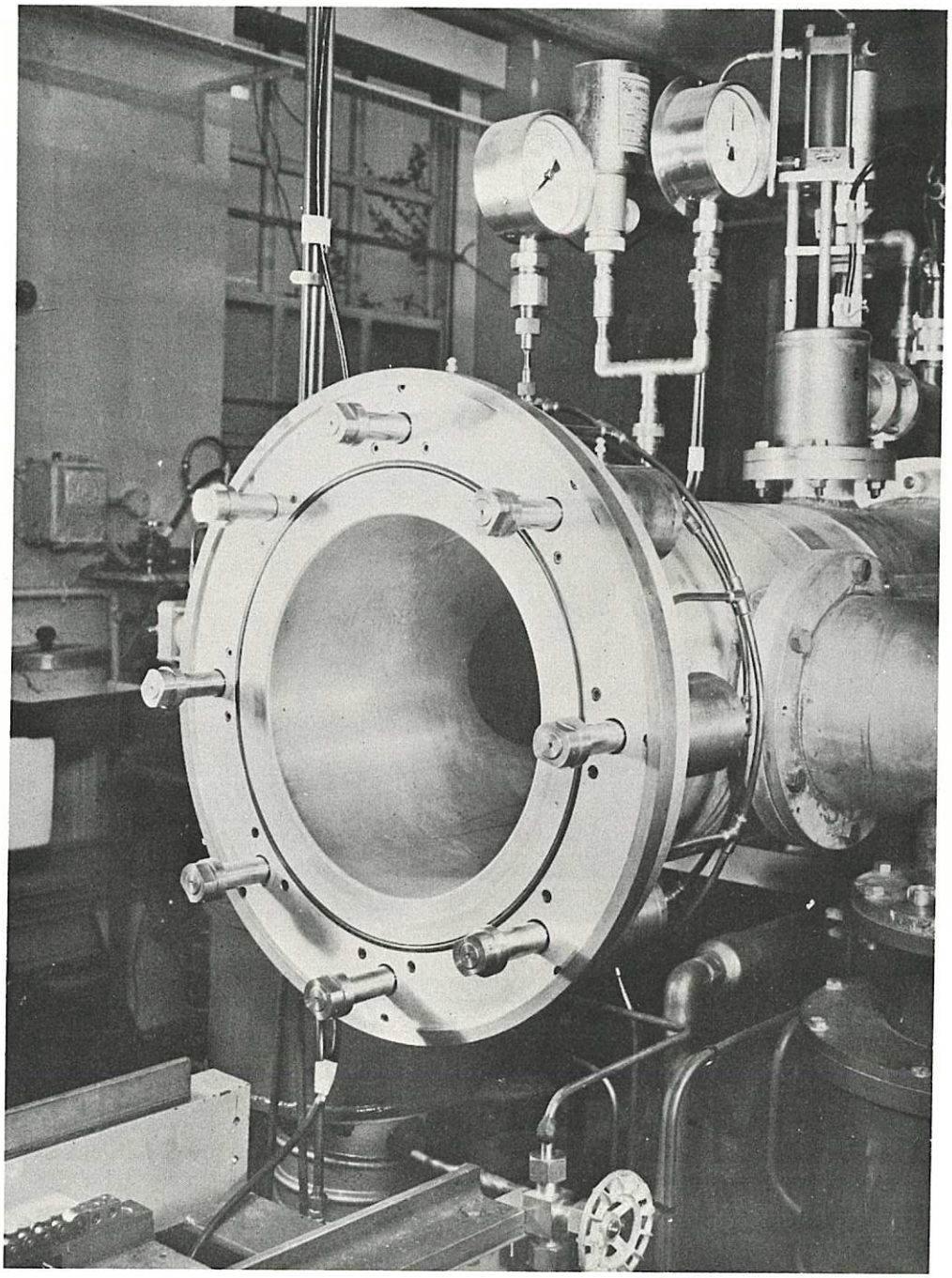

MOUTH OF EXPANSION CHAMBER

Plate 3.2. To obtain this picture, the hydraulic clamp (see Plate 3.1) was unlocked and the compression chamber withdrawn along its tracks (the ends of which are visible at bottom left). In this position, the 0 ring diaphragm seal and all eight clamp units can be seen. The dark area about a foot along the tube from the mouth is part of one of the high vacuum valve seats, shown in the closed position.

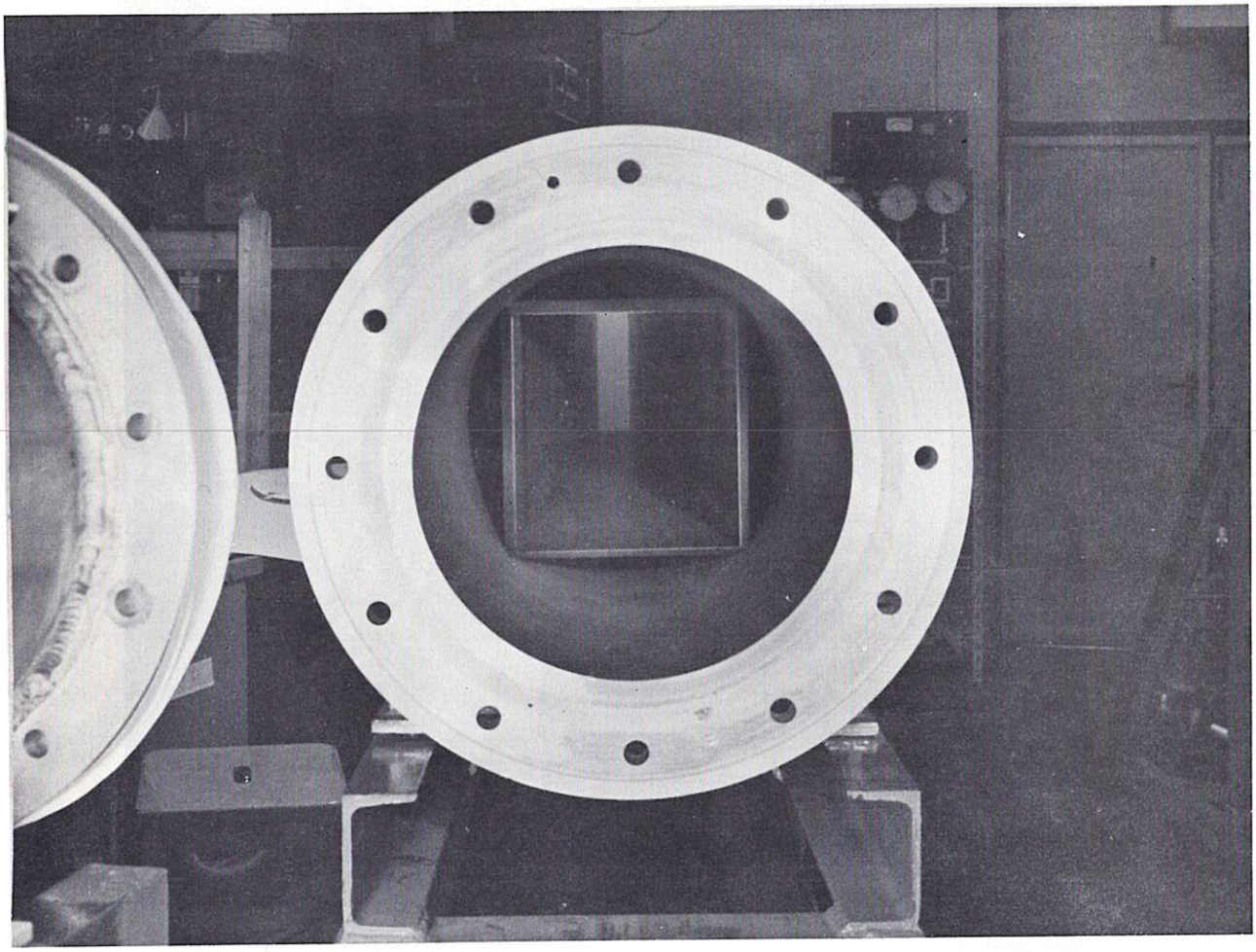

MOUTH OF CONVERGING CHANNEL

Plate 3.3. For general perspective and dimensions, refer to Fig. 2.1; the flange in the foreground is labelled A in that figure.

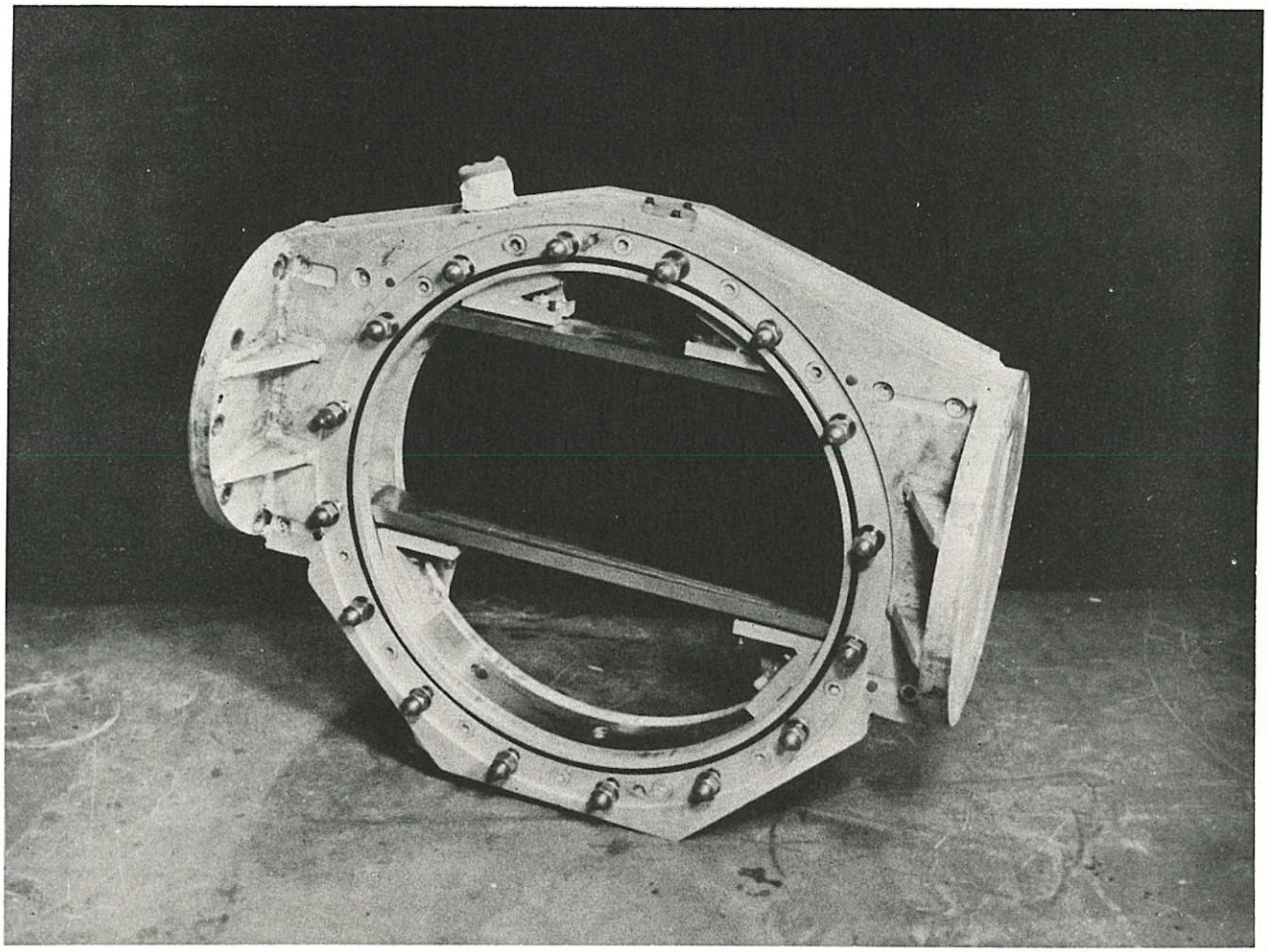

ILLUSTRATING CONSTRUCTION OF DIFFRACTION CHAMBER

Plate 3.4. The diffraction chamber is shown separated from the main tube. The windows having been removed in order to show the method of mounting the roof and floor bars.

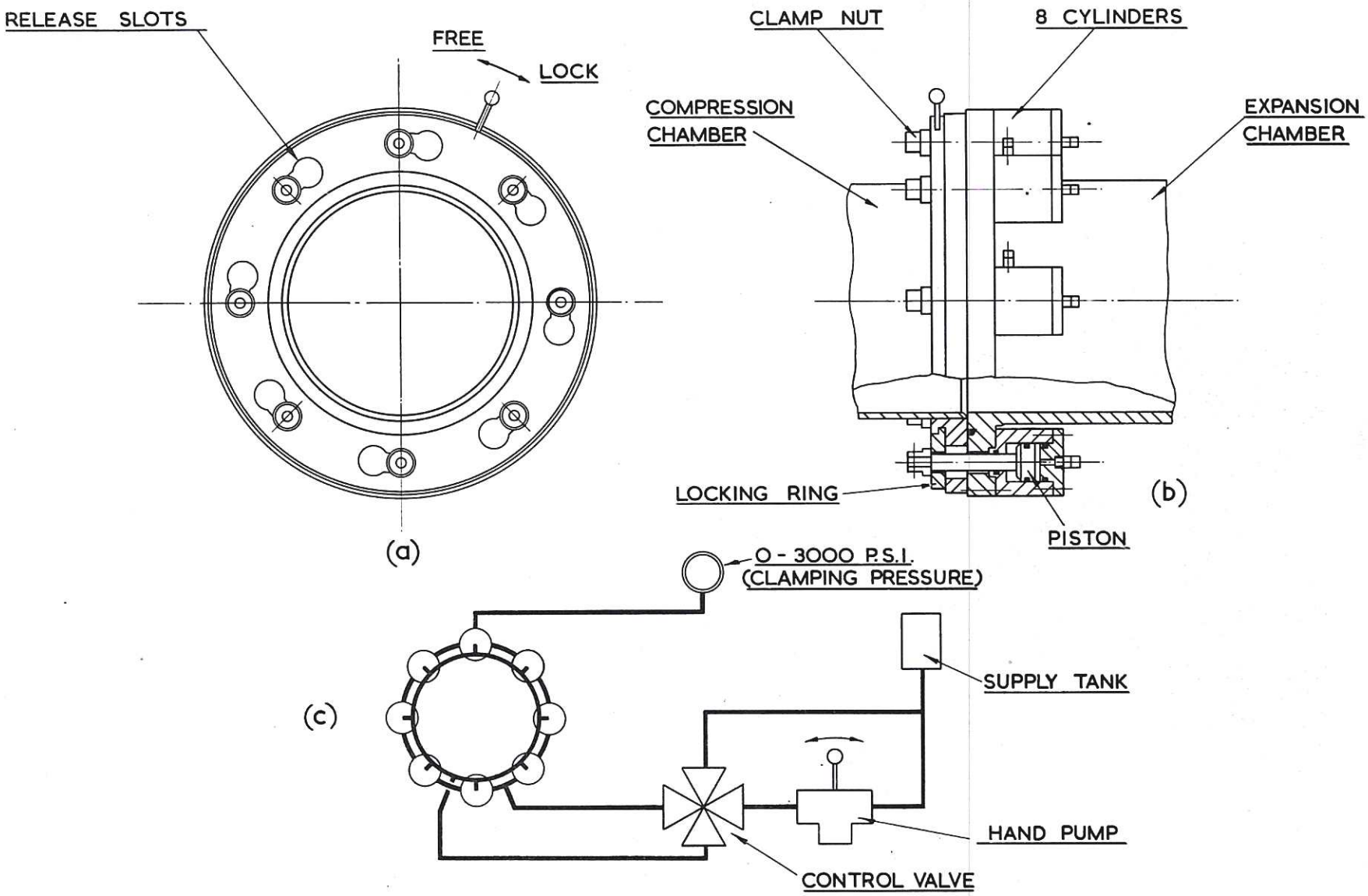

CLM-R18 FIG. 3·1. HYDRAULIC CLAMP OF DIAPHRAGM FLANGE. (SEE FIG. 2·1)

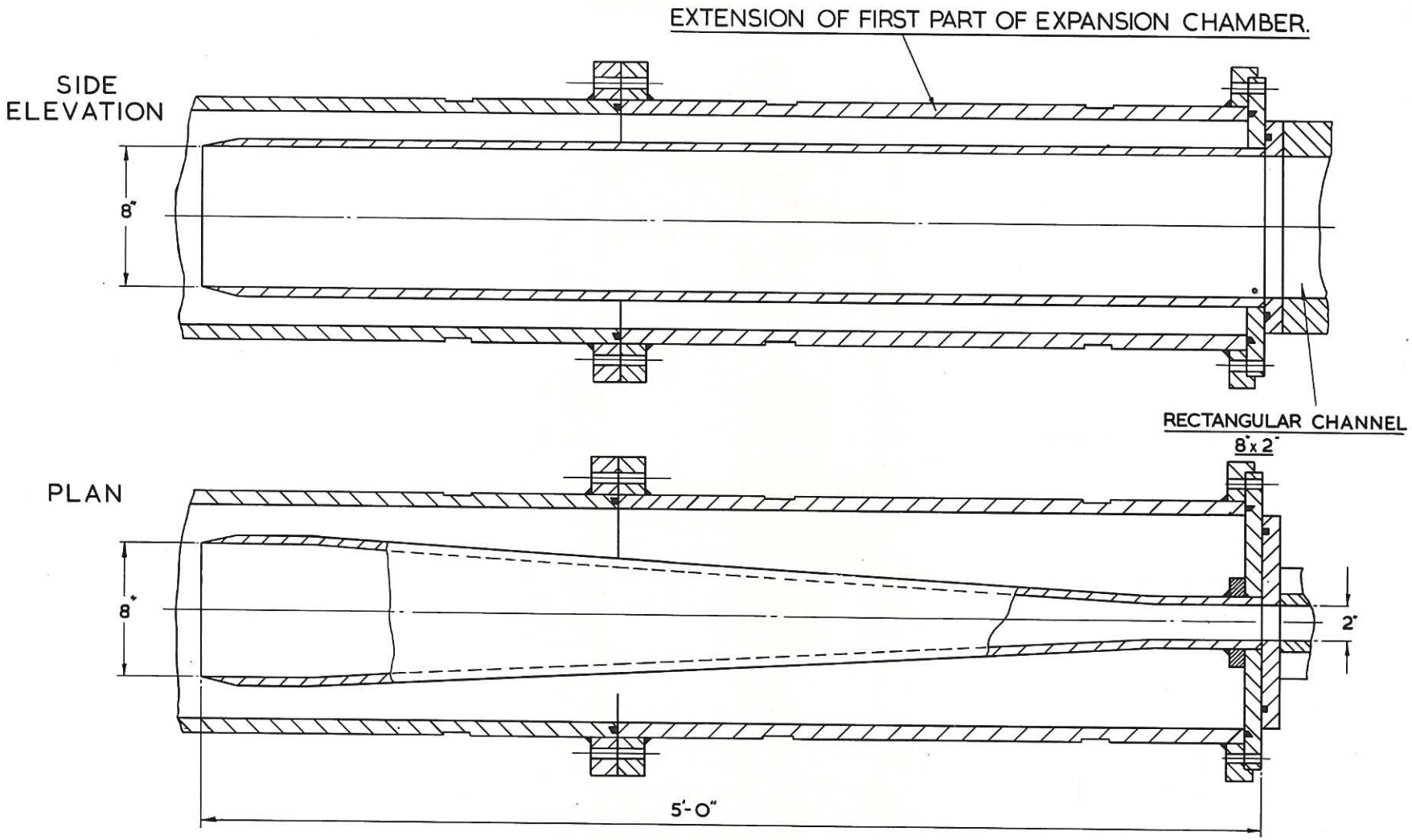

CLM-R18

FIG. 3·2. CONVERGING CHANNEL.

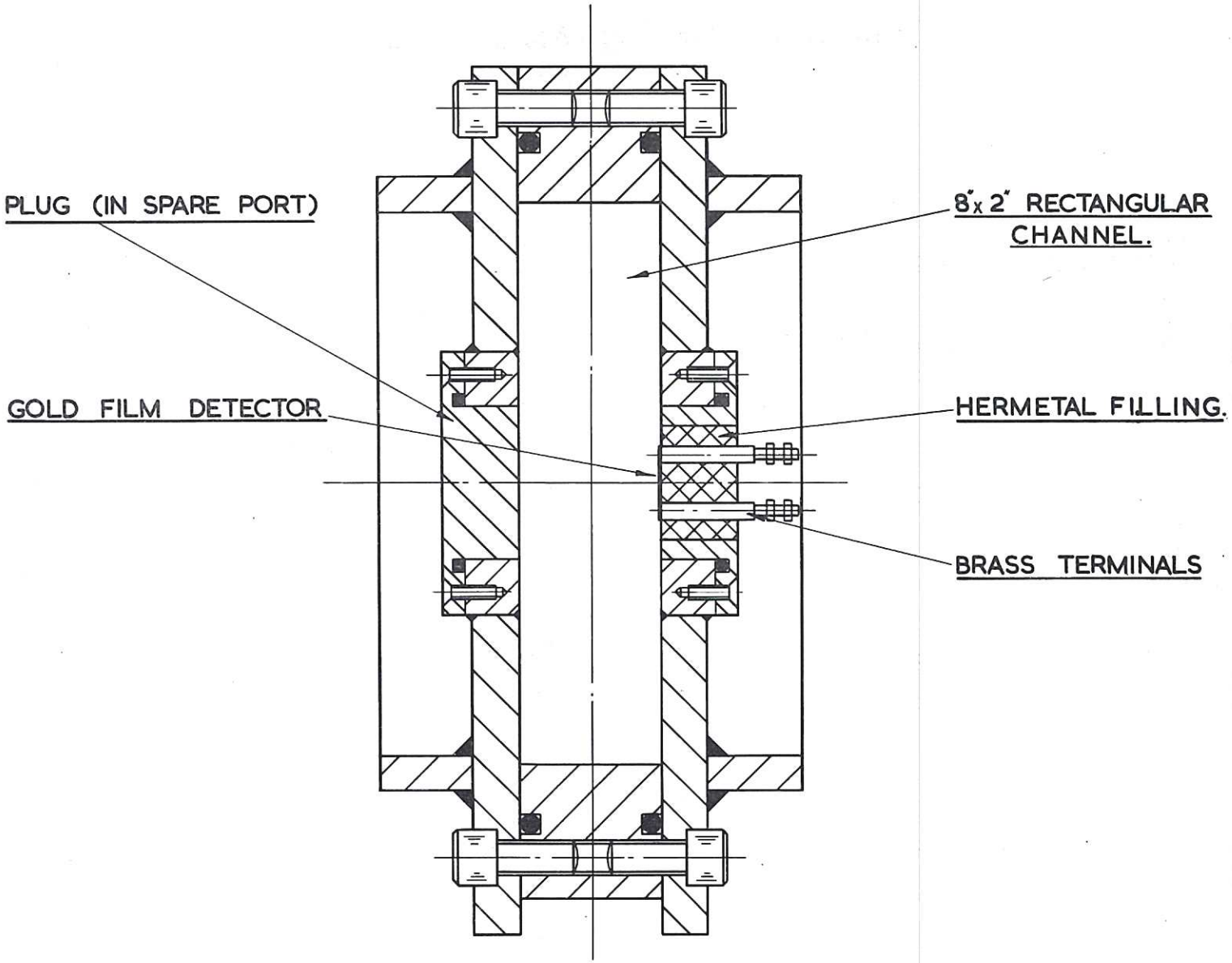

CLM-R18

FIG. 3·3. SECTION THROUGH DETECTOR STATION.

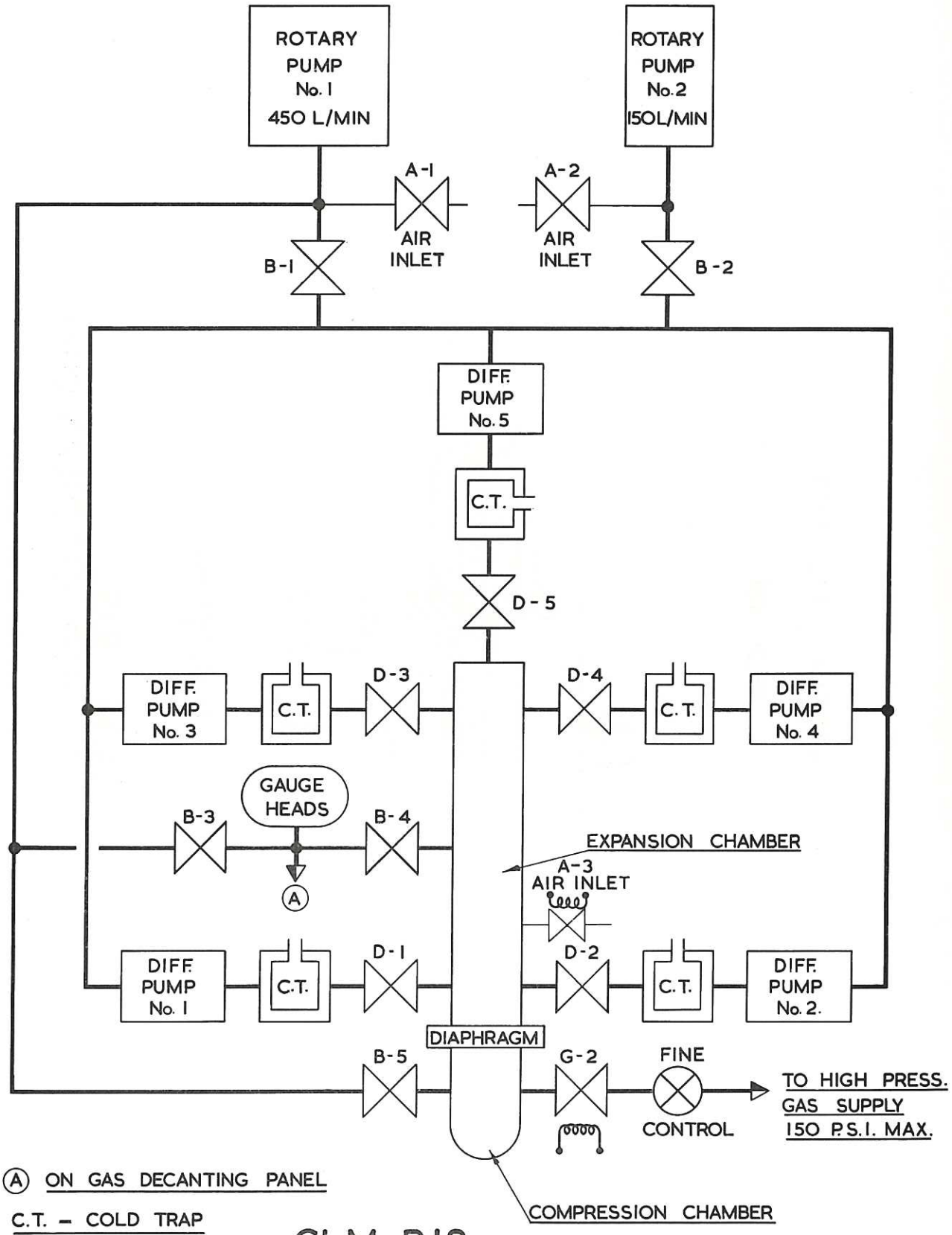

(A) ON GAS DECANTING PANEL

C.T. – COLD TRAP

CLM-R18

FIG. 3·4. VACUUM SYSTEM (SCHEMATIC.)

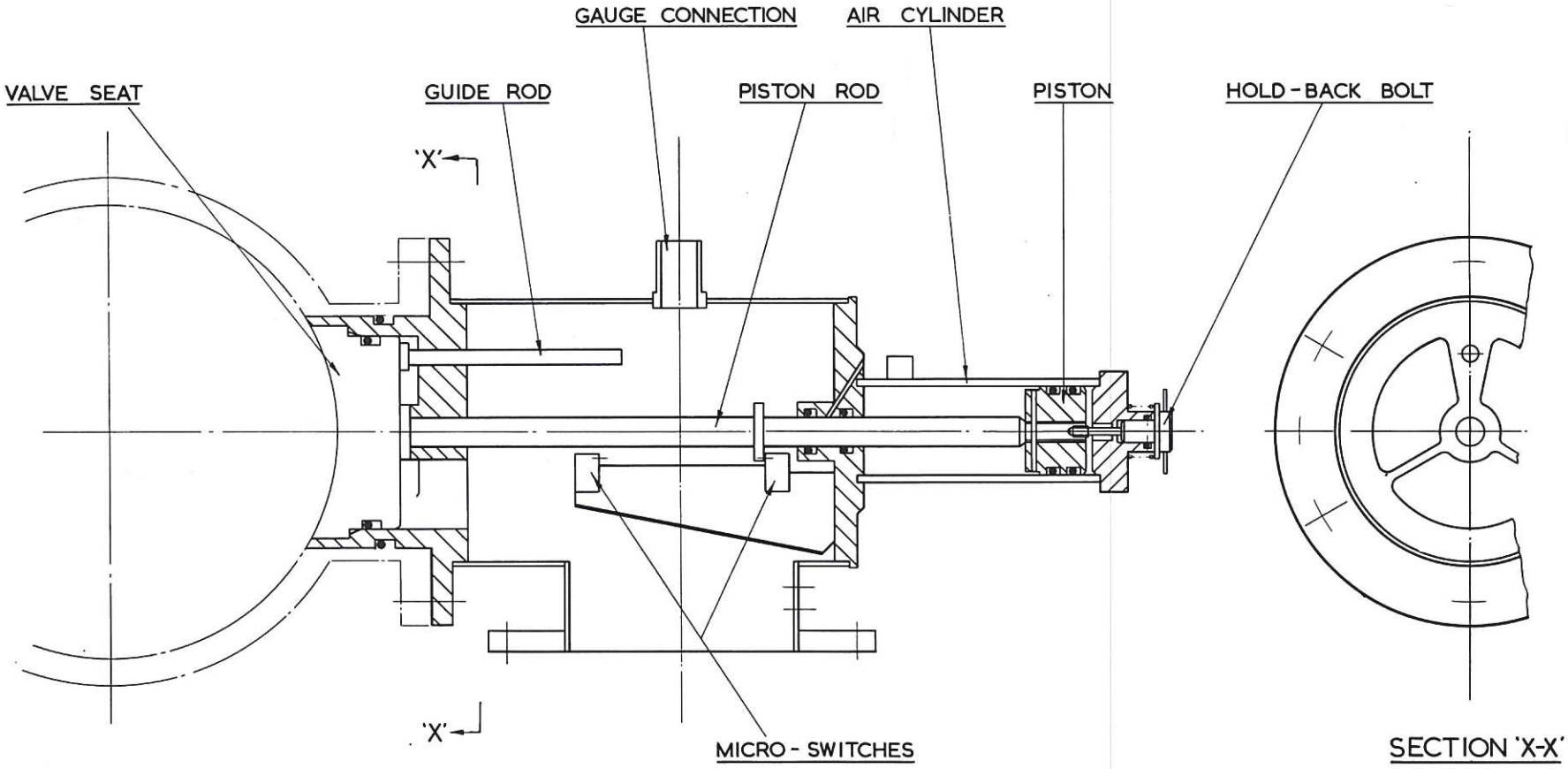

CLM – R18

FIG.3·5. VACUUM VALVE FOR CIRCULAR CHANNEL.

4. INSTRUMENTATION

Gas Decanting System

49. The desired range of p_1 was from 3 m.torr to 500 torr. The direct determination to 1 per cent or better of pressures less than 1 torr is a matter of some difficulty and we decided, therefore, to use an indirect method. The method we adopted was as follows. First a small vessel was filled to a relatively high pressure, which was measured to better than 1 per cent with a Bourdon gauge (which was periodically compared with a Fortin barometer). Then its contents were 'decanted' into the expansion chamber of the shock tube by opening valve G1 (see Fig. 4.1).

50. If y is the ratio of the volume of the small vessel, v, to that of the expansion chamber, V, and p^1 is the pressure of the gas in the small volume, then $p_1 = p^1 y$.

51. By successive filling of the expansion chamber via the small volume, until the final pressure in the expansion chamber was within the range of the Bourdon gauge, it was possible to determine y. If $\bar{p}_s$ denotes the pressure in the expansion chamber after s fillings and p_s is the pressure in the small volume prior to the s^{th} filling, then

$$y = \frac{\bar{p}_n - \bar{p}_o}{\Sigma_1^n p_s - \Sigma_1^n \bar{p}_s} \qquad (4.1)$$

when n is the total number of fillings.

52. It was convenient to have the choice between two small vessels for which y was 10^{-3} and 10^{-2} respectively, and one of three Bourdon gauges reading up to a maximum of 1, 3 and 14 atmospheres respectively.

53. Because of the wide range of conditions over which the shock tube was designed to operate, the effect of 1 per cent error in p_1 was variable. M depends strongly on the ratio p_4/p_1 when this is only slightly greater than one, but hardly at all when it is large. However, the effect of one per cent error in p_1 on the determination of M was always less than errors in timing the shock speed (see below).

Measurement of Shock Speed

54. The shock speed was obtained from measurements of the time taken for the shock front to pass two detectors fixed a known distance apart in the wall of the tube. Two types of shock detector were used, namely, an optical 'micro-schlieren' system and later, gold film thermal transducers. A different amplifier was used for each type of detector but otherwise the electronics was identical. For clarity, Fig. 4.3, a schematic diagram of all the electronic instrumentation, has been drawn showing only the gold film detectors. The amplified voltage signal produced by the passage of the shock front over the first, or upstream detector, opened a 'gate' to allow a stream of pulses, generated at one microsecond intervals by a crystal oscillator, to pass through to two 'scalers' connected in series. When the shock reached the second detector another pulse closed the 'gate'. Thus the 'scalers' recorded the time, in microseconds, for the shock to pass between the two detecting stations.

55. The accuracy of the shock speed measurements was determined by the crystal oscillator whose pulses were 0.5 microsecond wide and spaced 1.0 microsecond apart. To use this time resolution the response of the detector and its amplifier had to be equal to or better than 1.0 microsecond. The maximum

possible error was two microseconds which corresponded to an accuracy ranging from 0.1 per cent at M = 1 to 4 per cent at M = 14 in air, and somewhat greater in lighter gases.

'Microschlieren' System

56. In this method, described in reference (8) the abrupt change in refractive index associated with the increase in gas density at the shock front is used to reflect a beam of light as the shock passes and thus alter the current in a photomultiplier. A beam of light traversed the shock tube through windows 1 inch in diameter placed in opposite walls of the tube, so that the emergent beam was focussed on a vertical knife edge situated in front of a Mazda 27M2 photomultiplier. This knife edge could be inserted from either side of the emergent beam so that the amount of light falling on the photomultiplier either increased or decreased at the passage of the shock front. The intensity of illumination could be controlled by moving the knife edge in front of the beam.

57. The photomultiplier amplifier, whose circuit is shown in Fig. 4.8, had an overall gain of 30, which was sufficient to provide the 3 volt pulse required by the trigger circuit, and a response time of 0.25 microsecond. Three adjustable factors determined the sensitivity of this system, namely, the position of the knife edge in the light beam, the high tension voltage on the photomultiplier and the setting of the attenuator in the output of the amplifier. It is desirable to use the lowest high tension voltage possible to prolong the life of the photomultiplier.

58. This detecting system cannot be used satisfactorily at values of p_1 less than 10 torr; the exact value of the starting pressure below which the change of density at the shock front is too small to give rise to an appreciable signal depends on the shock strength and the nature of the gas.

Gold Film Detectors

59. To detect shocks for which $p_1 < 10$ torr use was made of the gold film thermal transducer method. This device has been described in detail by Blackman[18] and Price[5]. In our case the transducer element consisted of a thin film of gold, some two hundred atoms thick (5×10^{-5} mm) deposited on a strip of plastic tape 0.05 millimetres thick. Elements were prepared by vacuum evaporation of gold on to a long strip of the tape which was then cut into short, narrow lengths 10 mm long and 1 mm wide, having an electrical resistance of approximately 50 ohms. The gold film element was mounted on the end of a plug of insulating material ('hermetal') which carried two brass terminals (see Fig. 3.3). Each end of the gold film overlapped one of the terminals to which electrical contact was completed by a dab of silver paint. The plug fitted into a hole in the side wall of the shock tube in such a way that no mechanical obstruction was presented to the flow, the gold film being flush with the tube wall and having its long sides parallel to the plane of the incident shock.

60. The film was heated by the passage of the shock so that its resistance R ohms was momentarily increased by an amount which was determined by the temperature rise of the film T^1 in ^oK, as given by equations 9 and 12 in the Appendix, and the temperature coefficient of resistance $\alpha(^oC^{-1})$ for the film[5][23]. Thus if a constant current I amperes was passed through the film then this change in resistance would generate a voltage pulse of amplitude V volts given by

$$V = I \alpha R T^1 \qquad (4.2)$$

Since I was constant V was only dependent on the change in resistance caused by T^1. Provided the response time of the film was short then T^1, and hence V, was dependent on the temperature and density of the shocked gas. For a gold film 5×10^{-5} millimetres thick this response time was 2×10^{-8} seconds (Appendix, equation 10). This time resolution was not fully used since an overall response time of 1×10^{-6} seconds was sufficient for measuring the shock speed. Later work, not described here, approached more closely the time resolution of the gold film.

61. The family of curves drawn in Fig. 4.9 shows the theoretical signal V against shock Mach number M for shocks in air in the pressure range $p_1 = 760$ torr to $p_1 = 7.6$ m.torr. These theoretical curves were obtained from equation 4.2 by substituting appropriate numerical values for the current through the film, its resistance and temperature coefficient of resistance, and then inserting the expression for the temperature rise of the film T^1 (Appendix, equation 8). The equation so obtained was further reduced by inserting values for the thermal constants of the gas (air) and the plastic material backing the film (Appendix, equation 12). The theoretical signal voltage V can now be expressed in terms of the temperature of the shocked gas T_2, the temperature of the unshocked gas T_1 and the density ratio across the shock front:-

$$V = (T_2/T_1 - 1)(\rho_2/\rho_1)^{\frac{1}{2}} \quad 1.45 \cdot 10^{-3} \text{ volts.} \qquad (4.3)$$

Values of T_2/T_1 and ρ_2/ρ_1 as a function of shock Mach number were obtained from the tables calculated by Lukasciewz[10] and inserted in equation 4.3 to give the theoretical curve in Fig. 4.9 for an initial pressure $p_1 = 760$ torr. Curves for lower values of p_1 were drawn using equation 12 of the Appendix where it is shown that V varies as $p_1^{\frac{1}{2}}$. Equation 4.3 is valid when (a) the thermal properties of the gas and the plastic backing material are independent of temperature, (b) if the signal amplitude V is measured before the signal has time to penetrate the backing of the film and (c) if the effect of gas flow is ignored[24]. More detailed treatment is given in the Appendix.

62. A sequence of experiments was carried out during which the amplitude of the voltage pulse from a gold film was measured for shocks in air in the pressure range $p_1 = 760$ torr to 7.6 m.torr. Each voltage pulse was displayed on an oscilloscope, photographed and its amplitude measured with an accuracy of $\pm$ 10 per cent. These experimental measurements are plotted in Fig. 4.9 and may be compared with the theoretical curves.

63. Figure 4.10 shows the gold film signal as a function of the temperature of the gas (air) behind the shock, using values tabulated by Lukasiewiz[10]. The signal voltages are normalised to a common density behind the shock front. The full line shows the theoretical variation of the signal with temperature T while the plotted points are those obtained from experimental measurements. There is considerable scatter among these points but the general trend over a pressure range of 10^5 can be seen.

64. The gold film signal is effectively in series with the voltage due to the 'thermal noise' of the resistance of the film. Thus the weakest detectable shock is that which produces a signal equal to the 'thermal noise' of the film. This limit may be extended by increasing the current passing through the film and to a lesser extent, by increasing the resistance of the film. The maximum current which the films could pass without burning out was 30 mA for a period of 10 minutes. By using these higher currents and increasing the length of the film to 20 mm, shocks in air as weak as $M = 1.07$ at $p_1 = 76$ torr and $M = 4$ at $p_1 = 7.6$ m.torr have been detected. The corresponding temperature rise of the film for these minimum detected shocks is approximately 10 ^{o}K.

The Gold Film Signal Amplifier

65. The amplifier circuit is shown in Fig. 4.4. To detect the weakest shocks which generate a signal of a few microvolts high gain was needed together with a low noise input circuit. In addition the amplifier bandwidth had to be wide enough to give a time resolution of 1.0 microsecond. These conflicting requirements were met by an amplifier with an overall gain of 10^6 and a bandwidth of 400 k c/s. To match the equivalent noise resistance of 1000 ohms of the first valve, a CV 455, with the gold film resistance, a pulse transformer with a step up ratio of 6:1 was inserted between the gold film and the grid of the first valve. Thus a film resistance of 55 ohms became 2000 ohms at the first grid. A damping resistance of 4700 ohms was connected across the secondary of the pulse transformer and this was effectively in parallel with the 2000 ohms reflected resistance of the gold film giving a resultant resistance of 1,400 ohms. Thus the total equivalent noise resistance at the grid of the first valve was 2,400 ohms. Since the effeective measured noise bandwidth of the amplifier was 400 kc/s the theoretical R.M.S. noise voltage at the first grid for a temperature of 293°K is 6 μV, or 1 μV at the film; this should be compared with the mean, 5.9 ± 1 μV, of eight measurements of this quantity by different methods. Thus a signal of a few microvolts should be sufficient to provide unambiguous triggering of any device connected to the amplifier. In practice spurious triggering due to sources of external interference limited the lowest consistently detected signal to 10 μV at the film, corresponding to 60 μV at the grid of the first valve.

66. The overall gain of the amplifier was variable from 10(20 db) to 10^6(120 db) in steps of 2 db by means of coarse and fine gain controls which enabled the gain to be set below the threshold of occasional triggering by noise. The gold film detector with its leads and transformer were carefully screened, particularly against mains interference, and to reduce microphony the first two valves were mounted on a sprung sub-chassis and enclosed in box. A cathode follower served as the output stage.

Trigger Circuit (Fig. 4.5)

67. This circuit converted the output signal from the amplifier to a pulse of sufficient amplitude to operate the 'gate' unambiguously even when the incoming signal only slightly exceeded the noise from the amplifier. This was achieved by using secondary emission pentodes[19] which respond only to signals above a sharply defined threshold.

68. In our circuit an E.F.P.60 was used and its output pulse amplified to 50 volts and fed through a cathode follower and fifty feet of cable to the gate circuit.

69. When a loudspeaker was plugged into the jack provided at the output of the cathode follower, trigger pulses could be heard. This enabled the gain of the amplifier (Fig. 4.4) to be adjusted conveniently by reducing it until the incoming noise just failed to actuate the trigger circuit. This facility was particularly useful when the expected signal was just greater than the noise.

Crystal Oscillator and Gate Circuit (Fig. 4.6)

70. This unit, which provides a train of pulses 1 microsecond apart, is basically similar to one developed at Manchester University[20]. Oscillations from a 1 Mc/s crystal oscillator are fed simultaneously to the grids of the valves V_3 and V_4 whose anodes feed equal and opposite currents into the primary winding of a pulse transformer. Under these conditions the current in

the transformer secondary winding is zero. However, when a 50 volt positive pulse is applied to the 'start' terminal, the thyratron V_2 conducts and the consequent fall of the screen potential of V_3 cuts this valve off. This destroys the balance of currents in the primary winding of the transformer and pulses then flow from the output. The arrival of a similar pulse at the 'stop' terminal cuts off V_4 thus terminating the train of pulses. Although a voltage pulse of 12V amplitude was capable of firing each thyratron, in practice, the time delay between the application of the pulse and the instant of firing was only negligible when the pulse amplitude was over 50 V. The rectifier across the transformer secondary converts the oscillatory signals to unidirectional pulses. The bulbs across the anode load resistance glow only when the thyratron valves conduct. This provides a visual check on the operation of the circuit.

The Toepler-Schlieren System

71. The underlying principles of the Toepler-Schlieren technique for studying gas flows are discussed in detail in reference (8). Briefly, a parallel beam of light produced by a light source placed at the focus of a concave mirror traverses the system to be studied. A second concave mirror brings this beam to a focus a short distance in front of the lens of a camera, which in turn is focussed on the image of the system, as reflected in the second mirror.

72. The beam focus will be sharp and a uniform patch of light produced at the focal plane of the camera, in the absence of any irregularity due to finite size of source, imperfections in the mirrors and optical inhomogeneities in the medium traversed by the light beam. The intensity of the patch can be controlled by placing a knife edge in the beam at the focus of the second mirror. The introduction of some optical inhomogeneity, due in our case to the density variations in the diffraction chamber associated with the passage of a shock wave, deflects that part of the light beam affected by the density variations. The deflected rays will either brighten parts of the illuminated field or will be cut off by the opaque knife edge so that dark areas will be formed. The camera image will therefore show the field of the density variations. Plate 4.3 shows a typical schlieren photograph of a shock in a curved channel[6].

73. The schlieren apparatus is illustrated in Fig. 4.2, and Plate 4.2. Referring to Fig. 4.2, the spark source was mounted on a cradle which was supported on the ends of a pair of cantilever arms. The height of the cradle above the floor could be adjusted by means of a screw at one end. The cradle carried a mounting for the spark source unit which, by means of ball bearings running in parallel slots, permitted sideways and fore and aft movement in one plane. For fine adjustment of the position of this mounting, adjusting screws, with knurled heads, were fitted.

74. The two schlieren mirrors stood on shelves rigidly attached to the walls of the laboratory. The mirror mounts were provided with appropriate screws and clamps for accurate alignment.

75. The camera, see Plate 4.2, which was specially constructed out of an old quarter plate ($3\frac{1}{2}$" x $4\frac{1}{2}$") reflex camera with a roller blind focal plane shutter, had an F 8 lens with a focal length of 81 centimetres. The image of the diffraction chamber on the photographic plate has a diameter of 3 inches. The camera was clamped to an optical bench which also carried the knife edge mountings. Owing to anastigmatic aberration, the image of the source was not localised around one point. Two line images, about two inches apart, were produced, one vertical and the other horizontal. This accounts for the presence of two knife edges rather than one (see Fig. 4.2). One of these knife edges intercepted the horizontal image and the other the vertical. In

practice it was found convenient to have the choice of the use of one of these knife edges, since the contrast of the final image was determined to some extent by the orientation of the knife edge with respect to the direction of density gradients in the gas flow under investigation.

76. Each knife edge was the edge of a slot cut in a square brass plate which was mounted on a special carrier clamped to the optical bench. It was possible to remove the brass plate without disturbing the carrier.

Alignment of the Schlieren System

77. It was first necessary to set the optical axis of each component in one plane perpendicular to the side walls of the diffraction chamber, and then the light beam had to be collimated and focussed. In carrying out these operations the spark source was replaced by a continuous light source (see Plate 4.1).

78. Alignment was facilitated by a plumb line, reaching from ceiling to floor and passing through the centre of the diffraction chamber. This line, together with its images reflected in the windows of the diffraction chamber, was viewed through a small aperture (1/16" diameter) in a metal plate supported on a stand in a position approximately below the camera lens. The position chosen was in the plane of the plumb line and its reflected image. The continuous source was moved transversely until it was obscured by the plumb line when viewed through the aperture.

79. A method described by Holder and North[8] was used to collimate the beam. This method makes use of the weak reflection from the first face of the diffraction chamber which results in the presence of a faint image of the source in the vicinity of the source. When by adjustment of Mirror A, this image coincides in position and focus with that of the source itself the beam of light produced by mirror A is parallel and normal to the windows of the diffraction chamber.

80. The alignment of Mirror B was effected by adjusting its orientation until the in-focus shadow of that portion of the plumb line which crossed the window, coincided with the out-of-focus plumb line shadow due to the line crossing the light path between Mirror B and the camera.

81. The image was then centred on the camera lens and screen and the knife edges adjusted for correct position at the focal points of the second mirror. The knife edges were moved along the beam until the circular image on the camera screen darkened uniformly as the edges were driven across the light path.

82. Correct camera focus was obtained by placing a fine jet of propane in the diffraction chamber of the shock tube and focussing on the schlieren image of the jet.

83. Finally, the spark source was brought into position to replace the continuous source and the system was ready for operation.

The Multiple Spark Light Source

84. The spark light source used (see Fig. 4.2 and Plate 4.1) was designed and built at A.W.R.E. Aldermaston, and has been described by Goodfellow[21] where complete details are given. It provided up to six successive sparks, each of one microsecond duration, from the main 'Libessart' spark gap, which was placed on a platform above a ring of six subsidiary trigatron spark gaps.

Each of the latter was provided with a modulator and they were arranged radially with respect to the main gap. The modulators were fired in turn by a sequence of six pulses, separated from each other by a predetermined interval and delayed so that all six occurred when the shock front was in the diffraction chamber. In most of our work, however, only one spark was required.

85. In operation a trigger pulse from one of the gold film amplifiers, is fed to a delay unit which provides a pulse, delayed by a desired amount, to actuate the six trigger generator. This latter unit provides six successive trigger pulses which fire the spark modulators.

86. Two identical delay units were fitted and could, when necessary, be used in series. Each unit could provide a delay of between 10 and 1,000 microseconds.

Trigger Generator for 6-Spark Modulator (Fig. 4.7)

87. This provided six pulses, each of 300 volts, which fired the spark modulators. Essentially the circuit comprises a square wave generator whose long output pulse (1 millisecond) switches on a Miller time base from which a linearly decreasing potential is applied simultaneously to the cathodes of six diode valves V_4A, B, C, D, E, F whose anodes are connected to points on a potential divider, so that each diode in turn begins to conduct when its cathode potential approaches that of its anode. Initiation of current in valve V_4A, supplies a negative voltage step to the control grid of valve V.5A, the first valve of a pulse generating circuit, which is one of six identical circuits served, in succession, with negative pulses by each of the diode valves V.4A, B, C, D, E and F. The time between consecutive pulses depends on the rate of decrease of the potential applied to the cathodes of the diode valves and this is determined by the time constant of the Miller time base valve V.2; in practice coarse control can be effected by choice of condenser and fine control by a means of a variable resistance. With this circuit it was possible to generate up to six pulses separated in time by intervals ranging from 4 to 200 microseconds.

88. The lower part of Fig. 4.7 shows the circuit of one of the six identical pulse generators which actuated the spark light source. The operation of the circuit is as follows. The valve V_5 is cut off by the arrival of a negative voltage step at its grid and the consequent rise in potential of its anode is transferred via a cathode follower V_6 to the grid of a thyratron V_7. The Thyratron then conducts and delivers a positive pulse of some 300 volts to the main spark modulator.

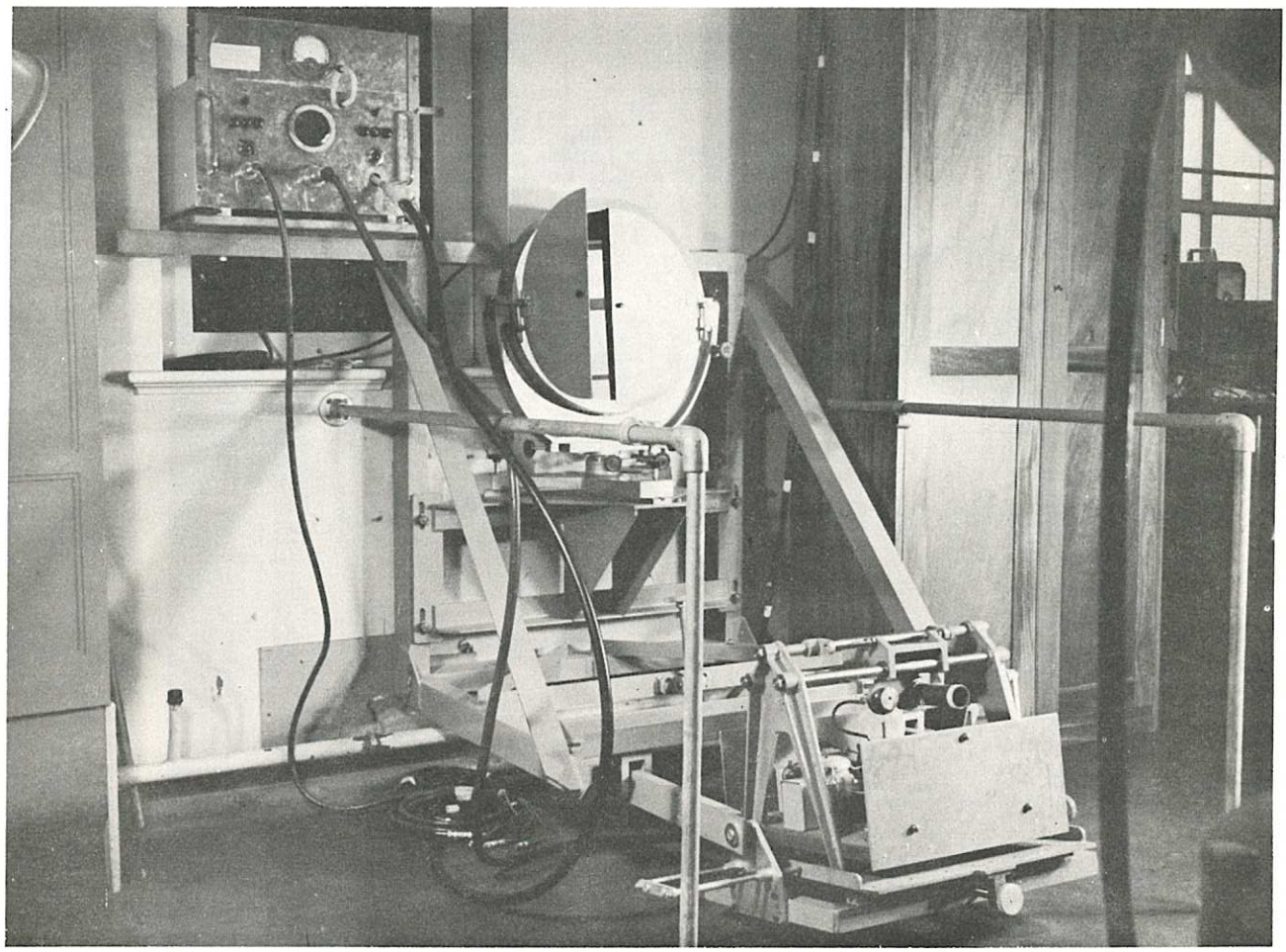

SCHLIEREN MIRROR 'B' AND SPARK LIGHT SOURCE

Plate 4.1. For perspective refer to Fig. 2.1. The schlieren mirror is shown with one of its semi-circular protective doors partially open.

The Libessart Spark Gap can be identified by the short H.T. cable leading down into the spark unit. Alongside it, supported on the same bridge structure, is a long copper cylinder containing the continuous light source used in aligning the schlieren system.

The spark unit is mounted on a cradle, the details of the construction and adjustment of which are given in Fig. 4.2.

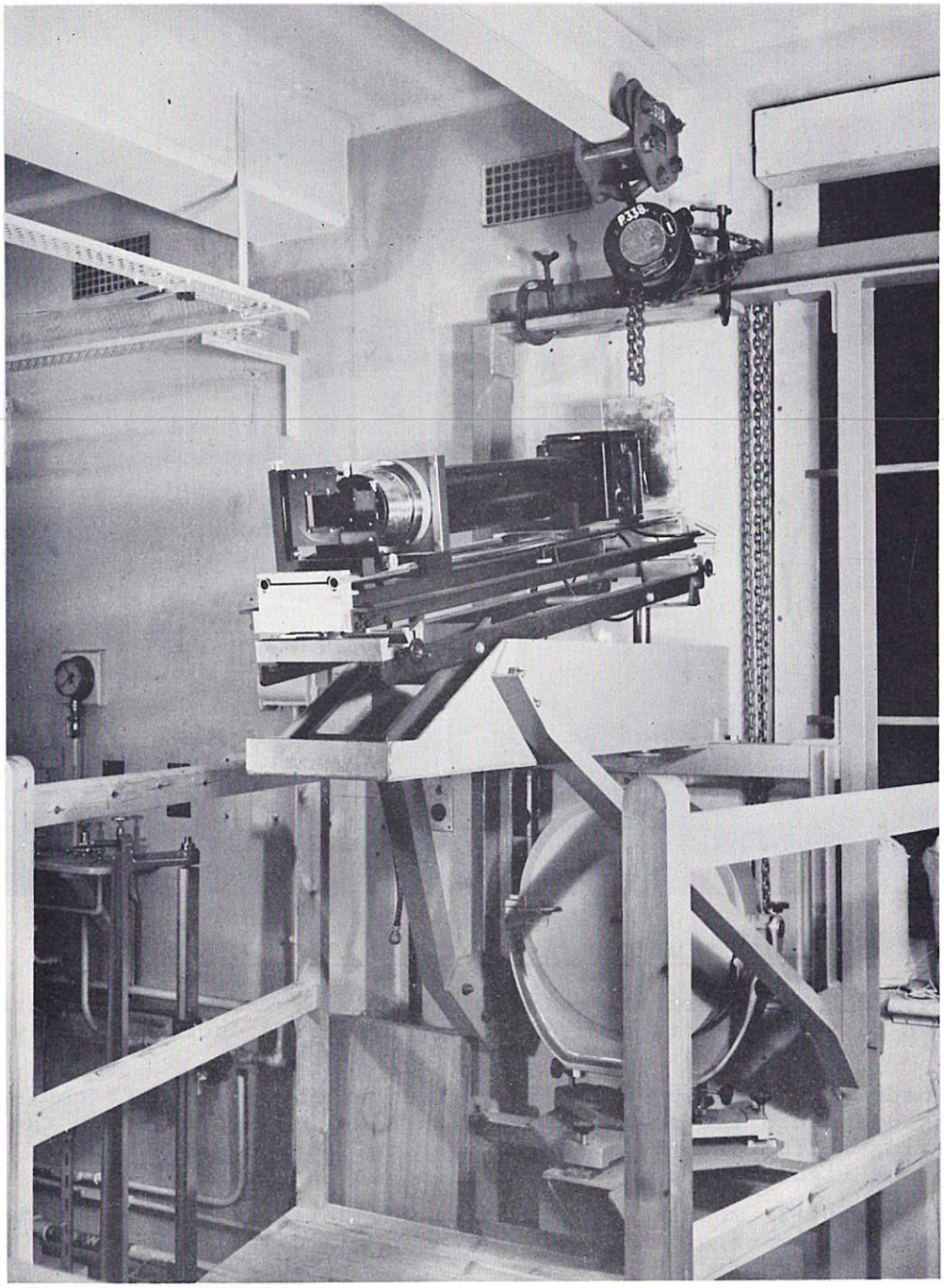

SCHLIEREN CAMERA AND MIRROR 'A'

Plate 4.2. The camera is shown supported on its adjustable frame, (for details of the adjustment of which see Fig. 4.2 and text), which rests on the rigid box shelf in the centre of the picture. In front of the lens are the two mountings carrying adjustable horizontal and vertical knife edges, the vertical knife edge being nearest the lens.

Below the camera is the schlieren mirror mounting. (see Plate 4.1).

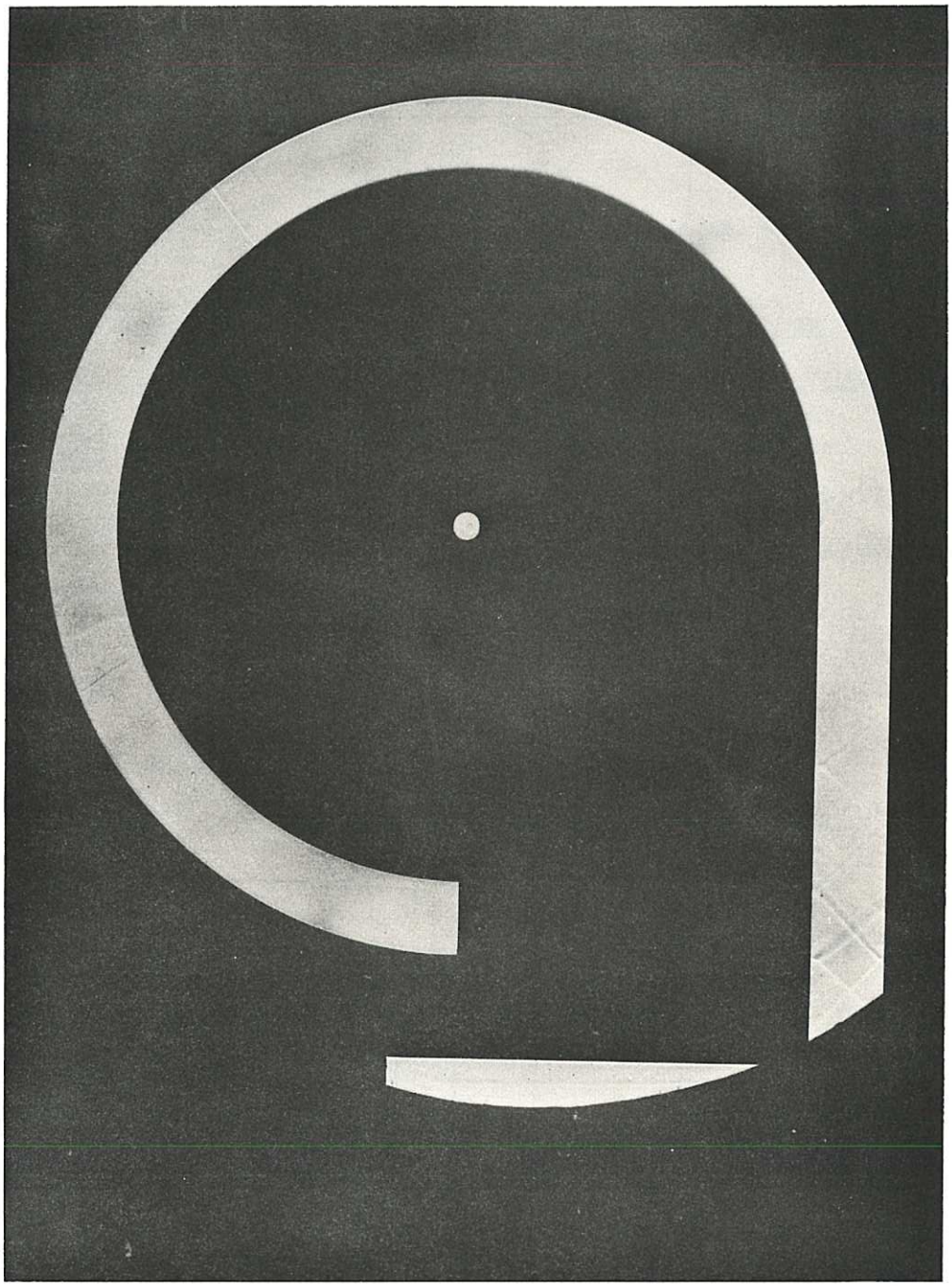

SCHLIEREN PHOTOGRAPH OF GAS FLOW BEHIND SHOCK IN A CURVED CHANNEL

Plate 4.3. The flow entered the channel at ~~top~~ bottom right, and the disturbance of the flow near the channel mouth is clearly seen. The angular distance of the position of the shock downstream of the entrance of the curved portion of the channel is 130°.

(Experimental details; Gas A; Air; Gas B; Argon. p_4 = 310 mm. Hg.; p_1 = 10 mm Hg. Shock Mach. Number 2.53)

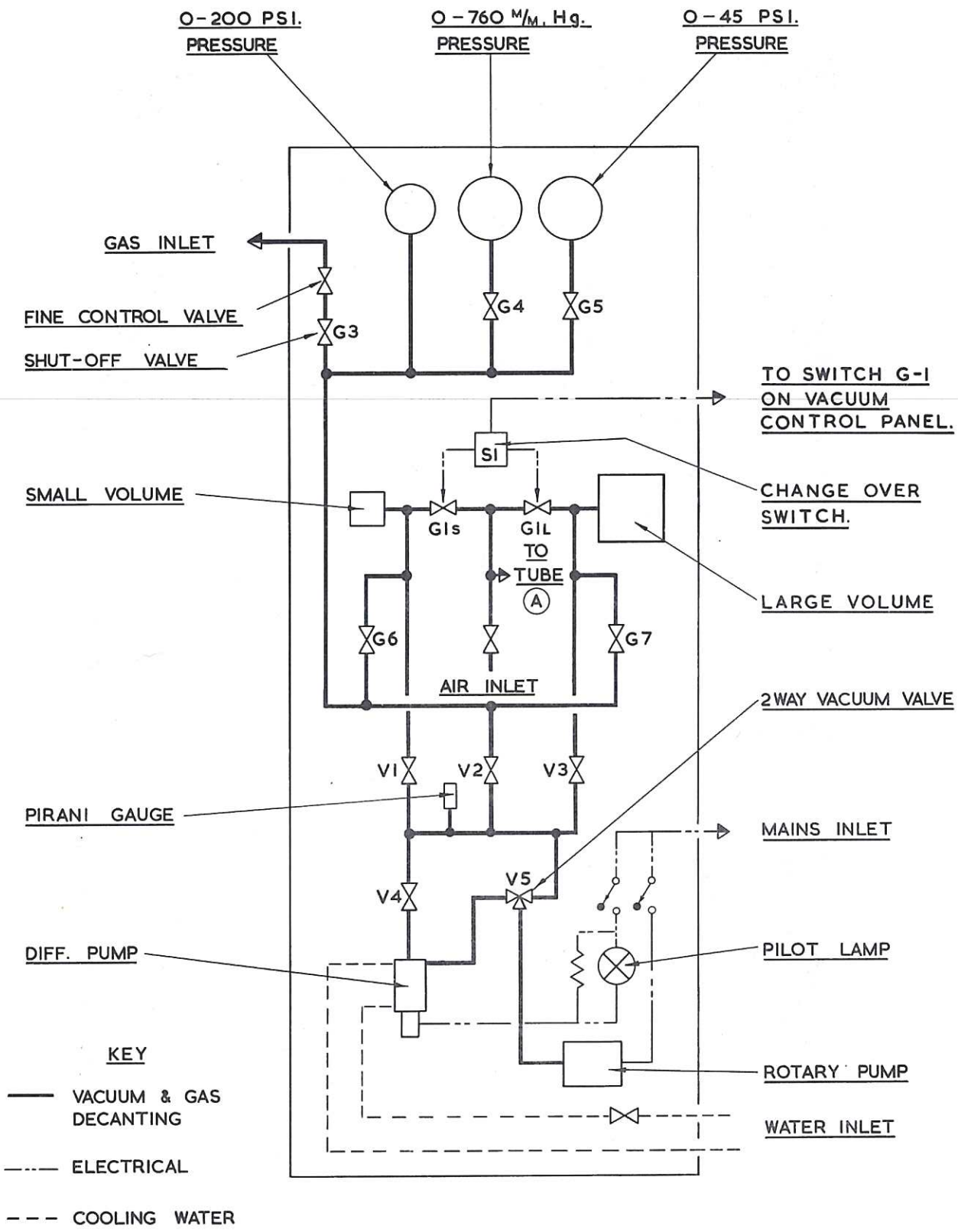

CLM-R18

FIG. 4·1. GAS DECANTING SYSTEM.

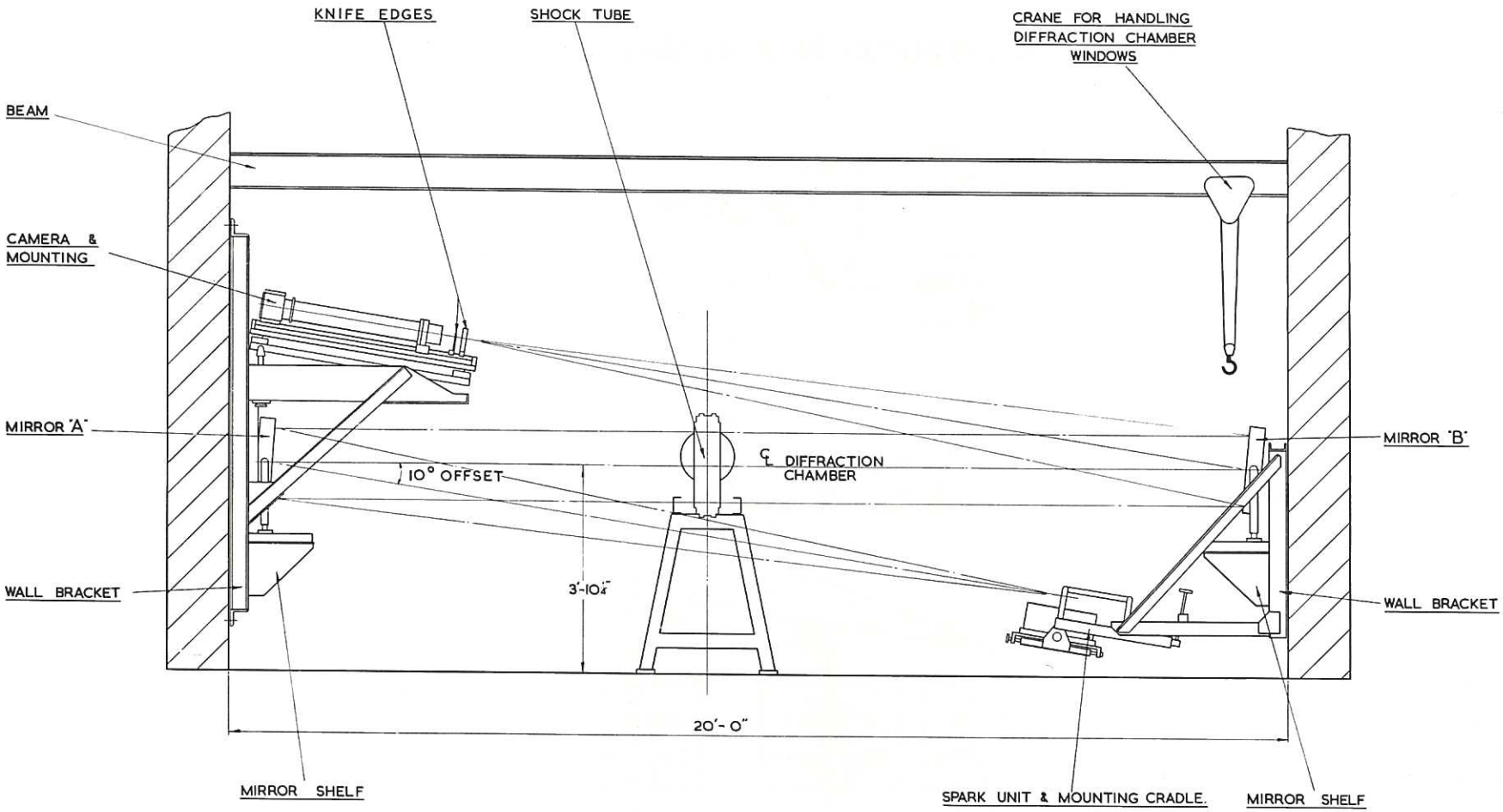

CLM-R18

FIG. 4·2. SCHLIEREN SYSTEM.

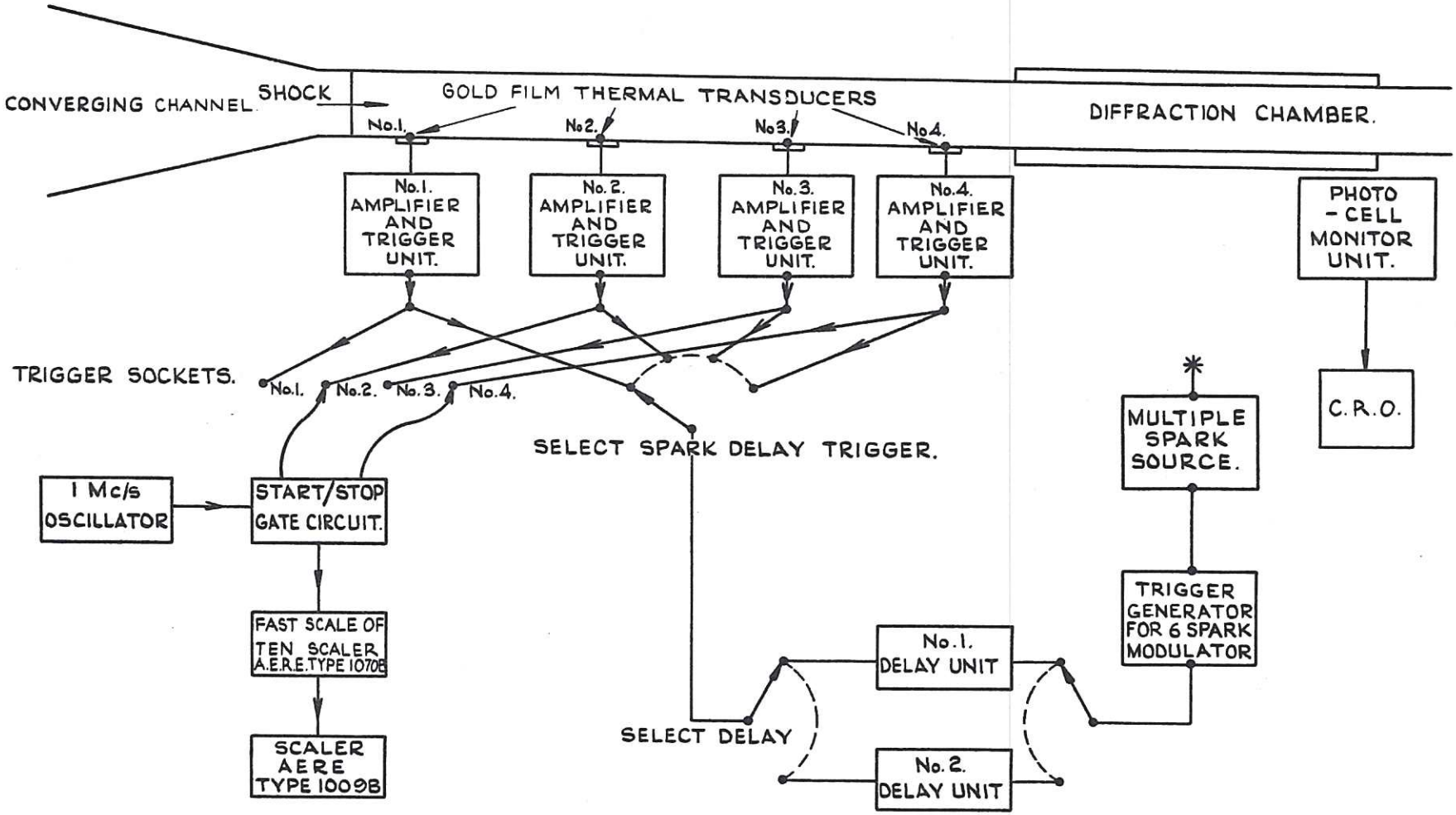

CLM-R18 FIG. 4·3. SCHEMATIC DIAGRAM OF ELECTRONIC INSTRUMENTATION.

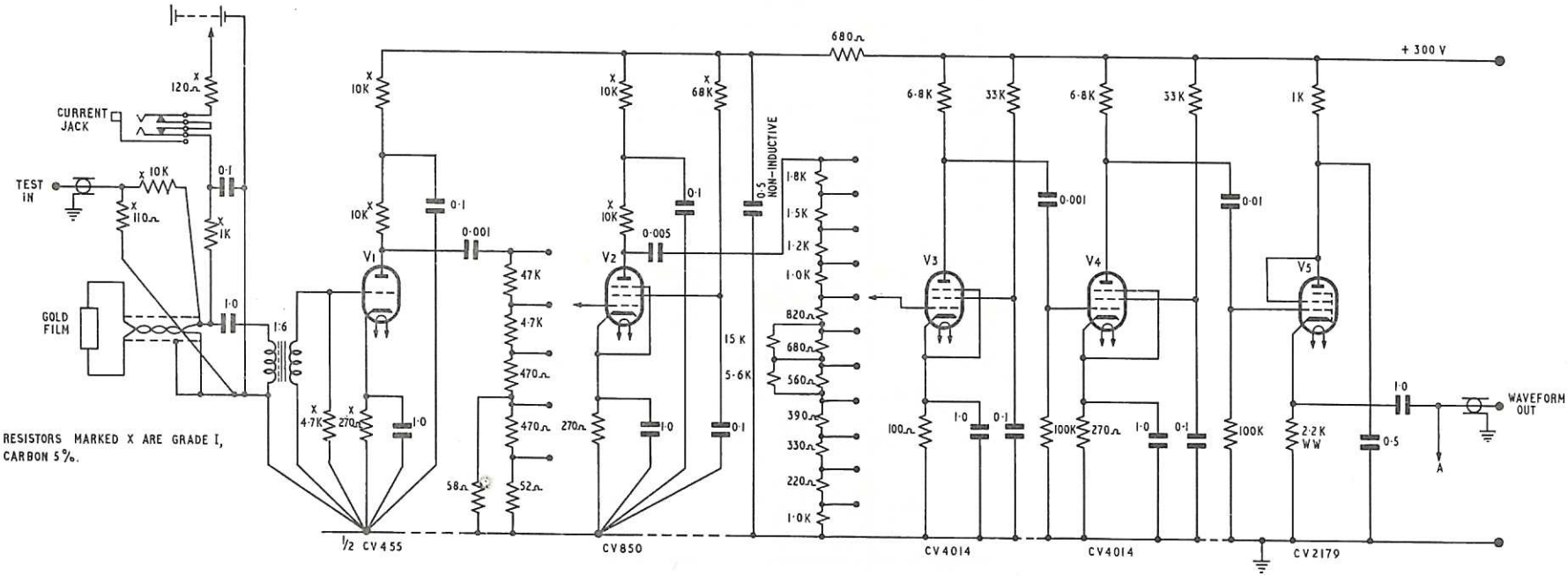

CLM-R18 FIG. 4·4. GOLD FILM SIGNAL AMPLIFIER CIRCUIT.

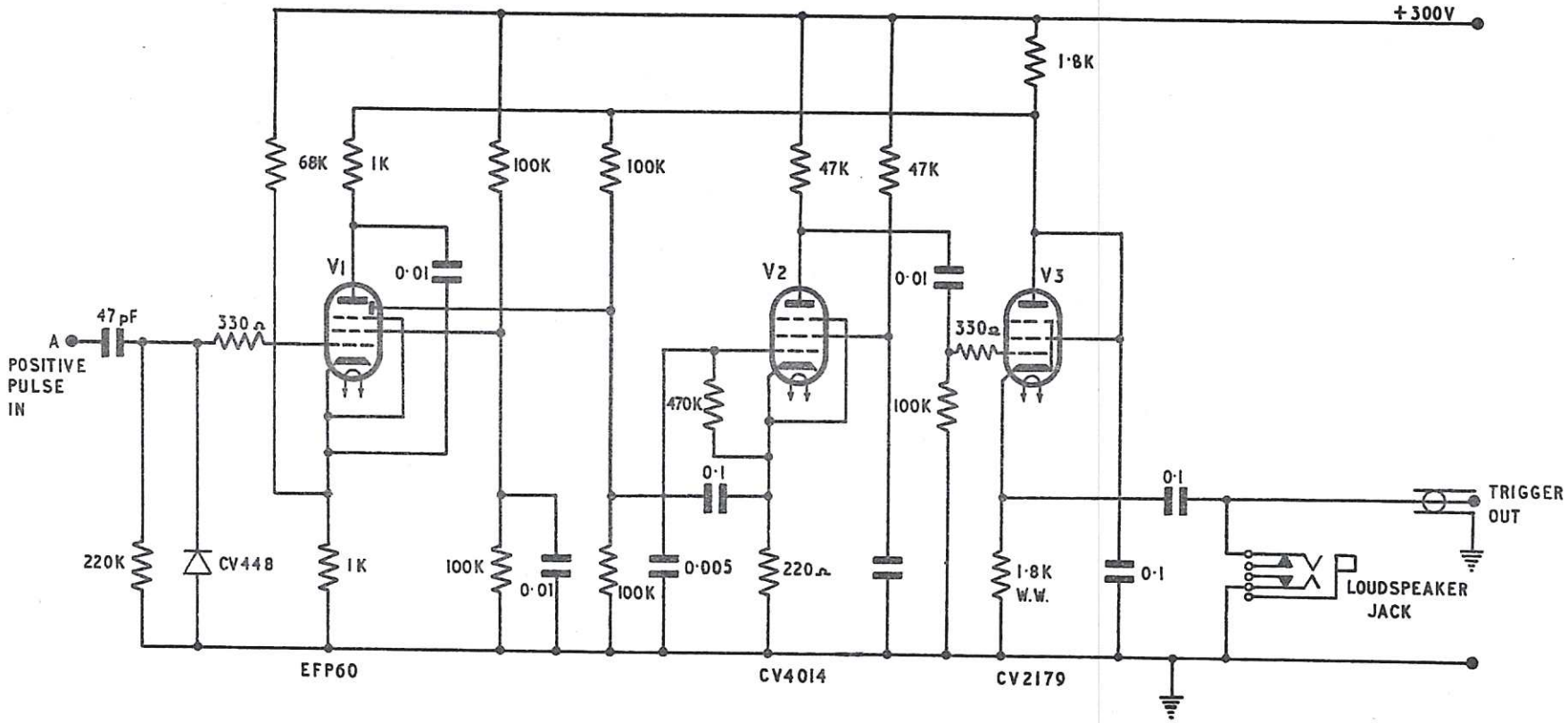

CLM-R 18. FIG.4·5. TRIGGER CIRCUIT.

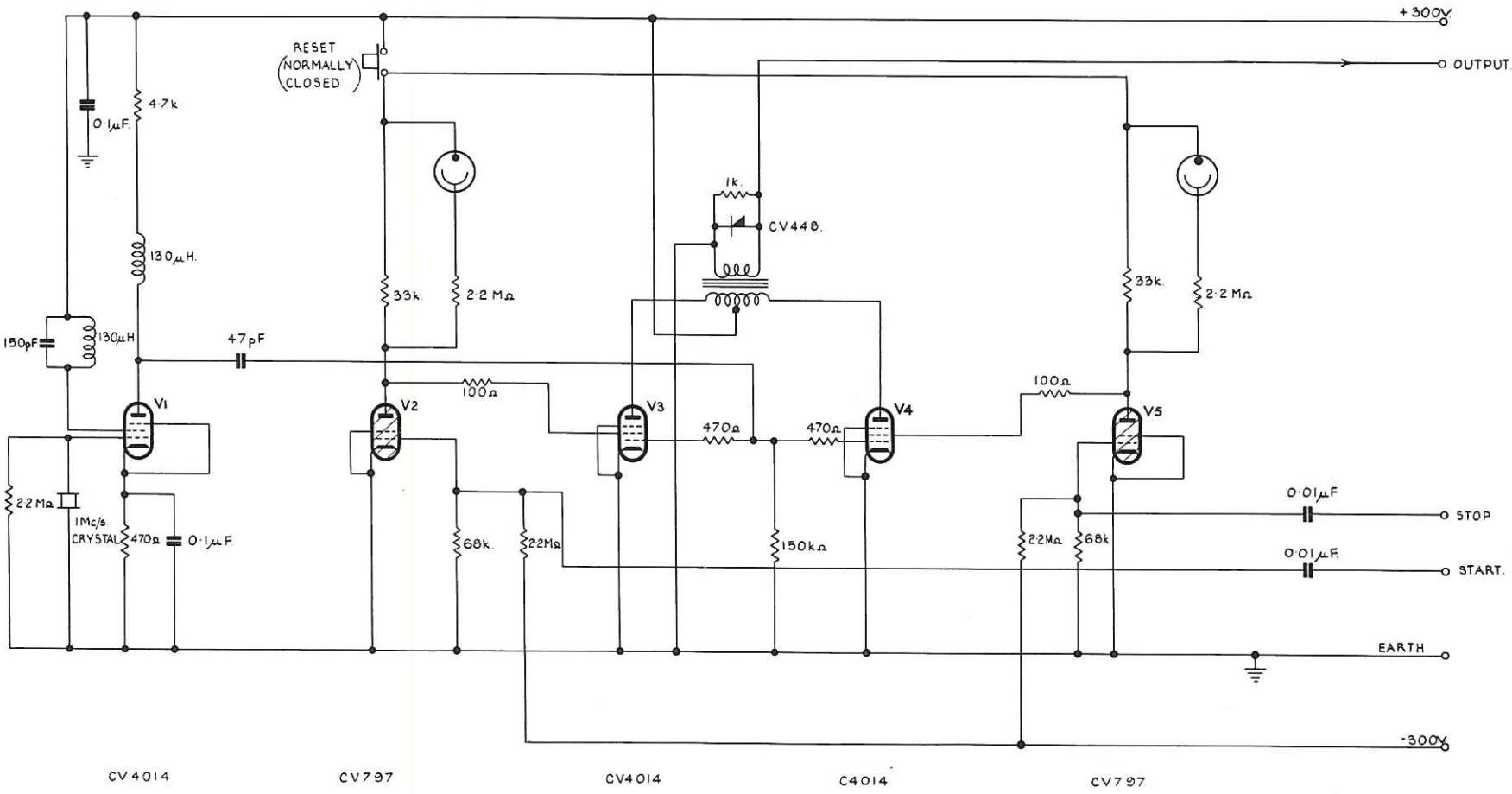

CLM – R18. FIG. 4·6. CRYSTAL OSCILLATOR AND GATE CIRCUIT.

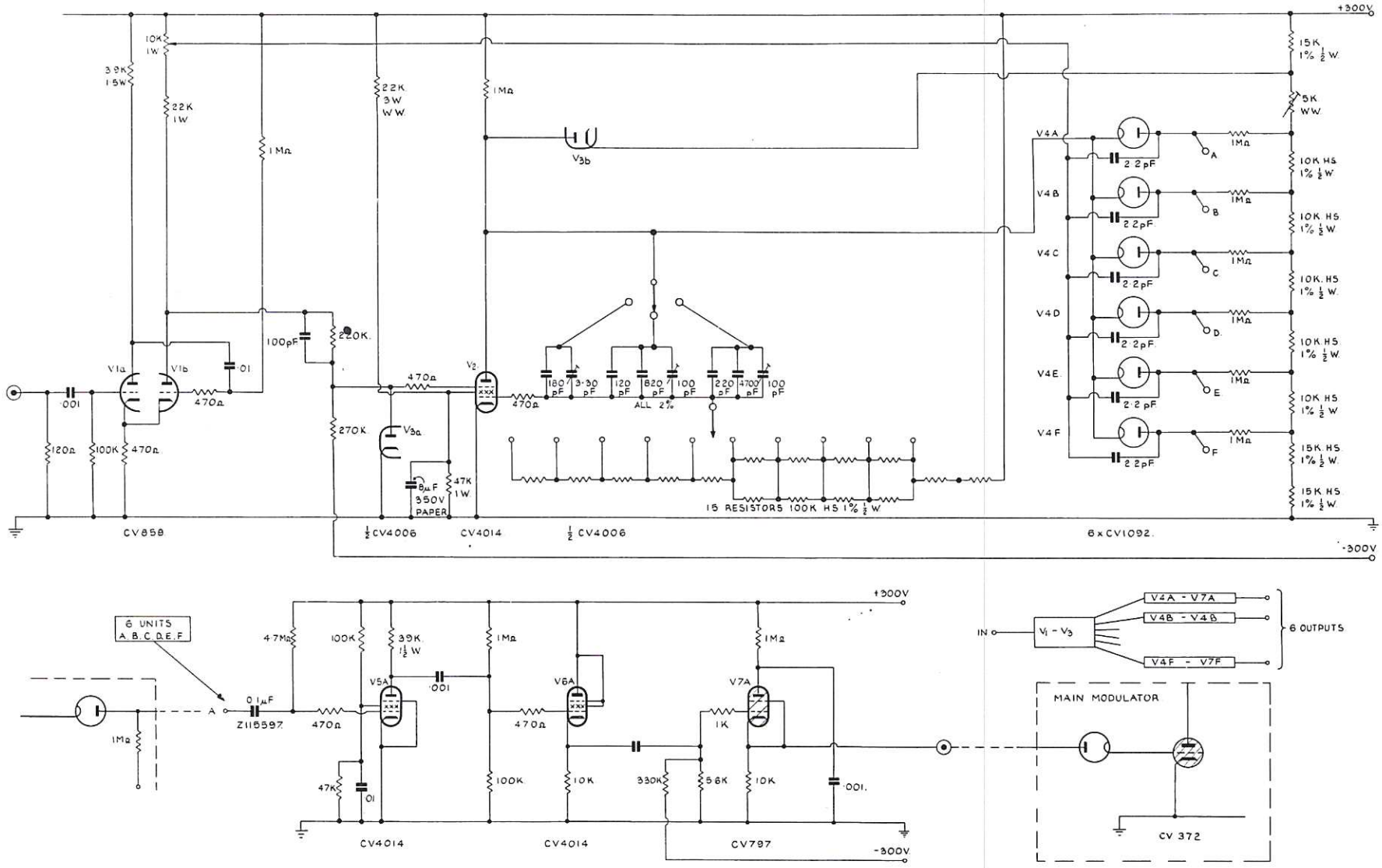

C L M – R 18 FIG. 4·7. TRIGGER GENERATOR FOR 6-SPARK MODULATOR.

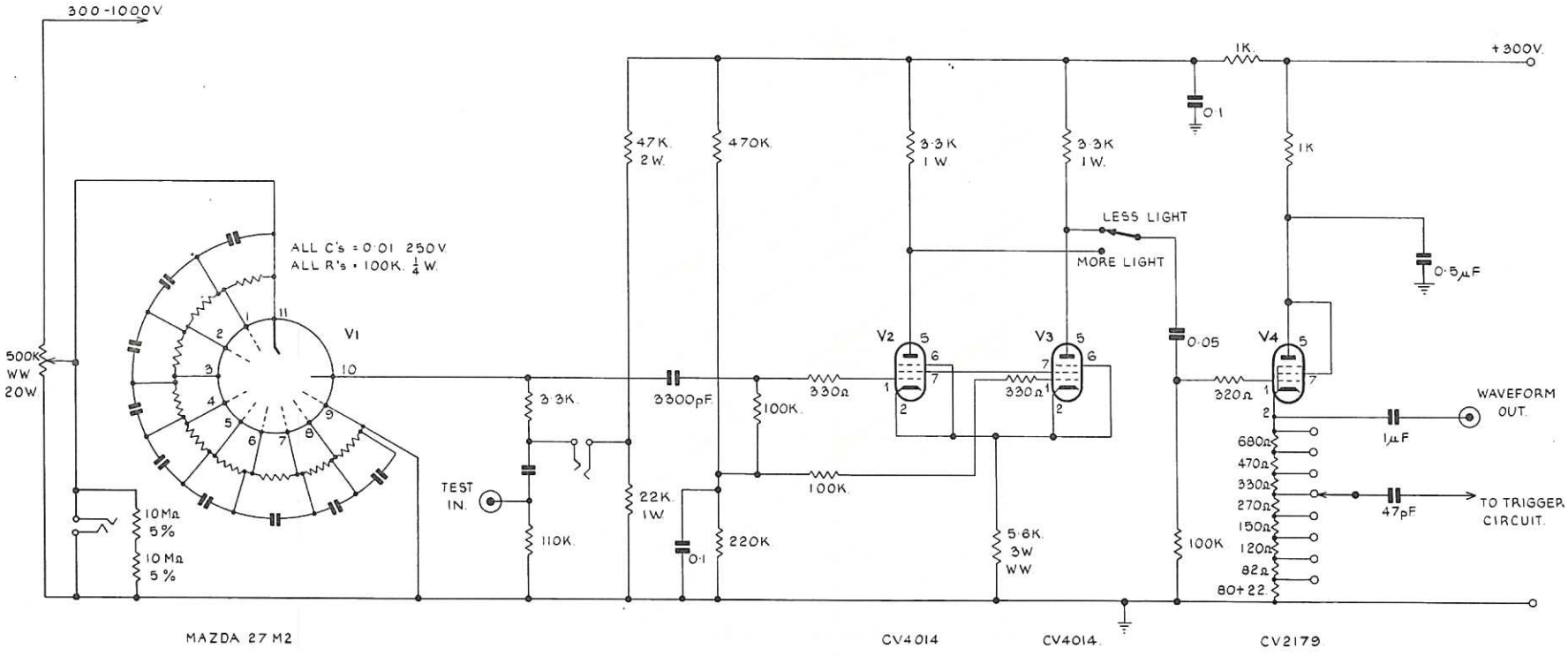

CLM. R18. FIG. 4·8.. PHOTOMULTIPLIER CIRCUIT.

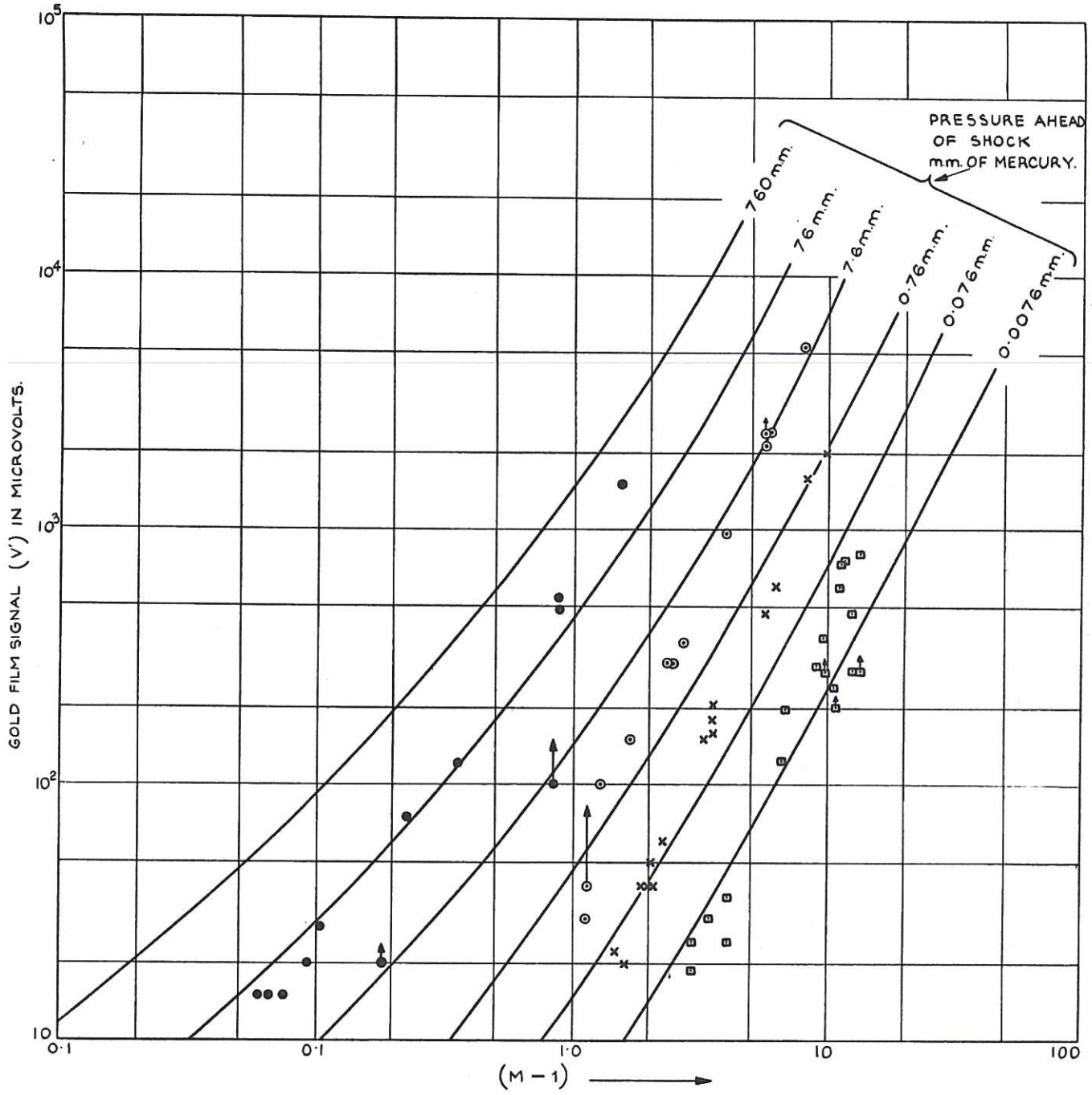

CLM-R18 FIG. 4·9. GOLD FILM SIGNAL AS A FUNCTION OF SHOCK MACH NUMBER FOR SHOCKS IN AIR.

CURRENT THROUGH FILM = 10 m.A.
RESISTANCE OF FILM. = 55 ohms.
ESTIMATED SIGNAL SHOWN THUS. —
THE POINTS REPRESENT EXPERIMENTAL DETERMINATIONS UNDER THE FOLLOWING CONDITIONS

PRESSURE RANGE (torr)			SYMBOL.
$2{\cdot}3 \times 10^{-3}$	TO	$2{\cdot}3 \times 10^{-2}$	⊡
$2{\cdot}3 \times 10^{-2}$	TO	$2{\cdot}3 \times 10^{-1}$	×
$2{\cdot}3 \times 10^{-1}$	TO	2·3	⊙
23	TO	230	●

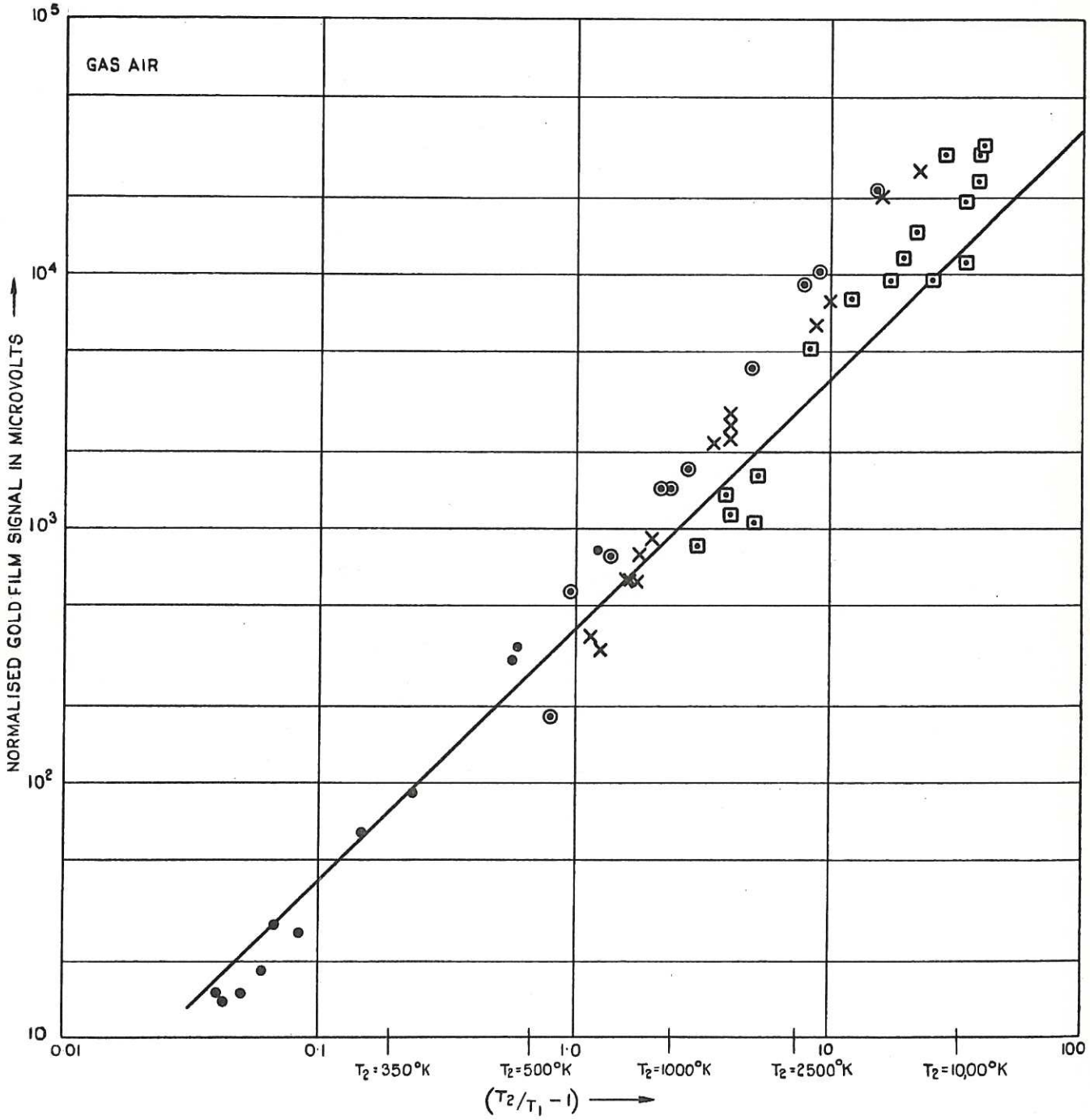

CLM-R18 FIG. 4·10. GOLD FILM SIGNAL AS A FUNCTION OF THE TEMPERATURE OF THE AIR BEHIND THE SHOCK.

T_1 = ROOM TEMPERATURE = 295°K
T_2 = TEMPERATURE OF GAS BEHIND SHOCK
ESTIMATED SIGNAL SHOWN THUS ——
ALL SIGNALS "NORMALISED" TO A PRESSURE OF 76 mm. BEHIND THE SHOCK (SEE TEXT)
THE POINTS REPRESENT EXPERIMENTAL DETERMINATIONS UNDER THE FOLLOWING CONDITIONS.

PRESSURE RANGE (torr)		SYMBOL
$2·3 \times 10^{-3}$	TO $2·3 \times 10^{-2}$	⊡
$2·3 \times 10^{-2}$	TO $2·3 \times 10^{-1}$	×
$2·3 \times 10^{-1}$	TO 2·3	◉
2·3	TO 230	●

5. CALIBRATION AND PERFORMANCE OF THE SHOCK TUBE

89. A complete test of the performance of the shock tube would involve (i) determining M, the shock Mach number, for the widest range available of gas combinations, A/B, pressure ratio, p_4/p_1 and temperature ratio T_4/T_1, (ii) making simultaneous determinations of p_2/p_1, ρ_2/ρ_1 and U_2 and (iii) making measurements of the duration of uniform flow behind the shock. In our calibration tests M was the only property of the shock to be measured. The highest value of p_4/p_1 attained was 5×10^5, and in all cases $T_4/T_1 = 1$. The gas combinations Air/Air, Air/Argon, Hydrogen/Argon, Hydrogen and Argon Mixture/Argon were used.

90. In estimating M, which is U, the shock speed, divided by $a_1 = (\gamma_1 RT_1/\mu_1)^{\frac{1}{2}}$ the speed of sound in the unshocked gas, U was obtained from the time τ taken for the shock front to pass between two gold film detector stations. Except at the lowest values of p_1 (see Figures given in this section) and, for reasons not properly understood, when hydrogen was used as the driver gas, the degree of reproducibility was very high indeed. Thus, for example, on those occasions when a number of shots were made under identical starting conditions the corresponding values of τ would agree to within $\pm$ 1 μsec which, as we have seen in section 4, is the best to be expected with the counting technique employed. This gave rise to the only significant uncertainty in M, which ranged from $\pm$ 0.2 per cent in the case of weak shots, to 4 per cent for strong shocks.

91. The results of the calibration tests are summarised in Figs. 5.1, 5.2, 5.3 and 5.4. In the first three of these diagrams, two curves are given, corresponding to the expected variation of M with p_4/p_1 given by equation (1.13) when assumptions (a)(b)(c) and (d) listed in para. 10 et seq. are valid (lower curve) and the variation of M with p_4/p_1 taking into account the expected amplification due to the converging section (equation 1.15), see para. 23 et seq. (upper curve). The upper curve gives the maximum expected value of M, since all deviations from the aforementioned assumptions will be associated with lower shock strengths. Such deviations should not be serious at sufficiently low values of M and high values of p_1, but at high values of M and low values of p_1, when so-called 'real gas effects' arise (assumption (d) no longer valid) and viscous friction and thermal conduction at the walls are no longer negligible (assumptions (b) and (c)), larger discrepancies can be expected[4].

92. Figures 5.1, 5.2 and 5.3 bear out these expectations. The results at low M and high p_1 (see Figs. 5.1 and 5.2) agree well with the upper curve, suggesting that under these conditions the flow in the shock tube is as visualized in para. 10. It will be of some importance to modify the theory given in that section to take account of deviations due to 'real gas effects' and then make a quantitative comparison with the experimental results at low values of p_1 and high values of M. This will be attempted in another report, where more extensive measurements using another shock tube of comparable dimensions will be combined with those given here.

93. Although the degree of reproducibility was generally high, small systematic errors, possibly due to imperfect diaphragm bursts, may have been present. A convenient technique for minimising the effects of such errors even when a wide range of M is required is to keep p_4 and p_1 fixed, so that the same diaphragm thickness can be used throughout, and vary μ_4 (see equation 1.13) by using a combination of two gases, one heavy and the other light, in the compression chamber, and varying the relative proportions of these gases. Thus, it was possible to obtain shocks in Argon at p_1 = 7.6 m torr ranging in strength from M = 3.5 by varying the relative partial pressure of Argon in the Argon/Hydrogen mixture in the compression chamber from 0 to 0.7 (see Fig. 5.4).

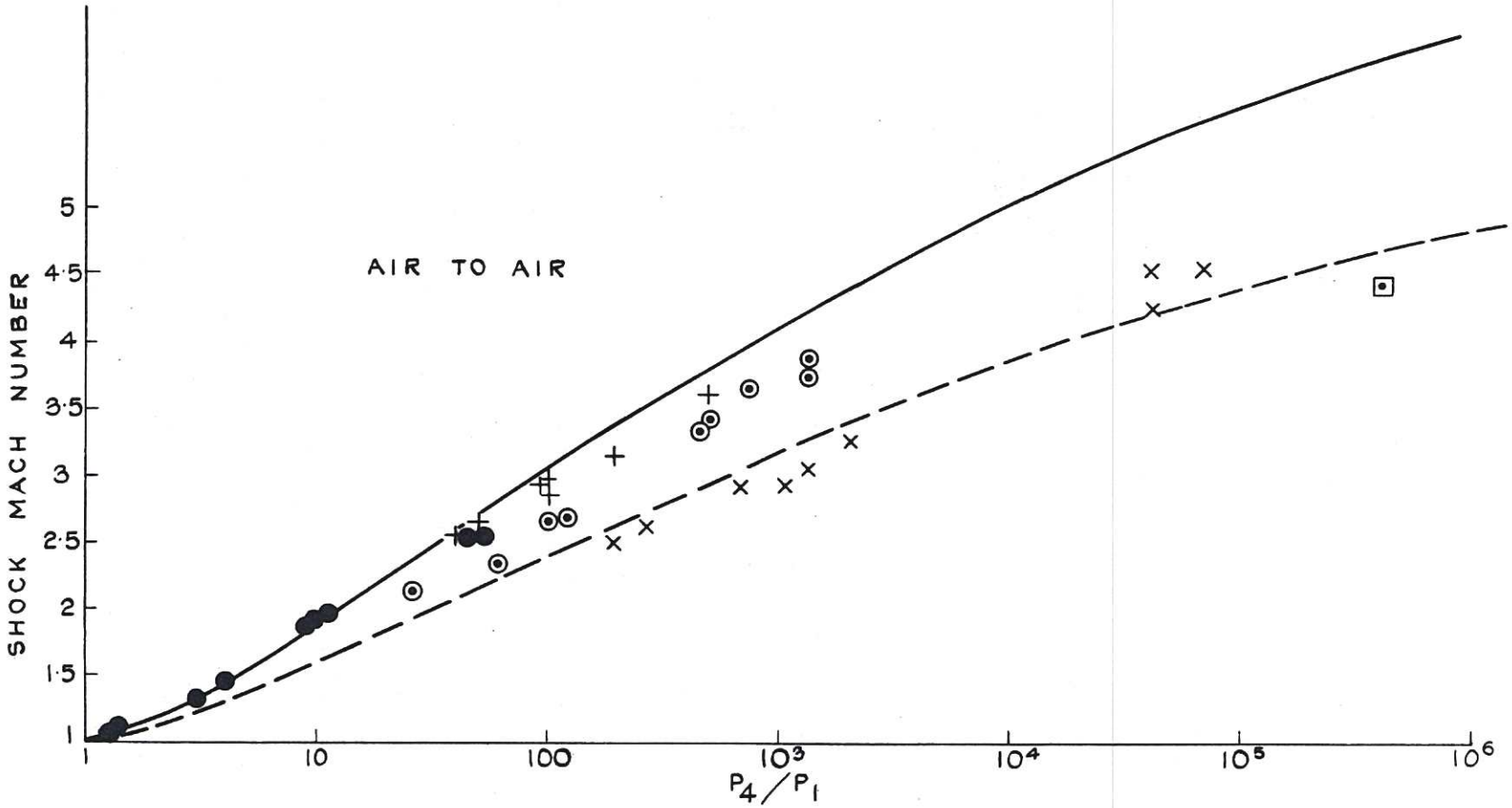

CLM-R18. FIG.5·1. SHOCK MACH NUMBER VERSUS P_4/P_1, FOR AIR TO AIR GAS COMBINATION.

THE POINTS REPRESENT EXPERIMENTAL DETERMINATIONS UNDER THE FOLLOWING CONDITIONS:-

PRESSURE RANGE (torr)		SYMBOL.
$2{\cdot}3\times10^{-3}$	TO $2{\cdot}3\times10^{-2}$	⊡
$2{\cdot}3\times10^{-2}$	TO $2{\cdot}3\times10^{-1}$	×
$2{\cdot}3\times10^{-1}$	TO 2·3	⊙
2·3	TO 23	+
23	TO 230	●

THESE SHOULD BE COMPARED WITH THE IDEAL FLUID THEORY, FIRST UNCORRECTED FOR THE EFFECT OF THE CONVERGING CHANNEL ---- AND THEN WITH THIS CORRECTION INCLUDED. ——

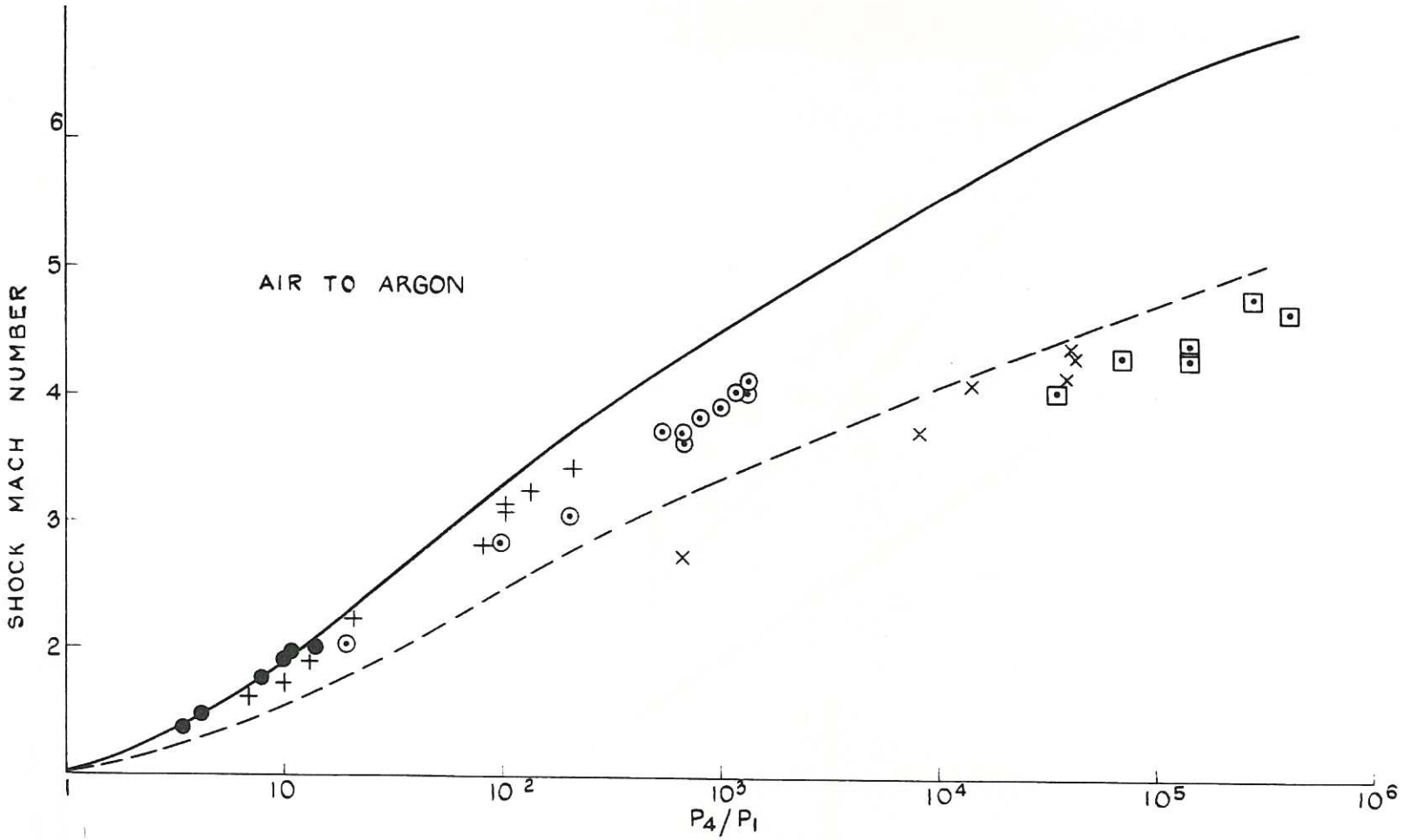

CLM-R18. FIG.5·2. SHOCK MACH NUMBER VERSUS P_4/P_1 FOR AIR TO ARGON GAS COMBINATION.

THE POINTS REPRESENT EXPERIMENTAL DETERMINATIONS UNDER THE FOLLOWING CONDITIONS:-

PRESSURE RANGE (torr)			SYMBOL
$2{\cdot}3\times10^{-3}$	TO	$2{\cdot}3\times10^{-2}$	⊡
$2{\cdot}3\times10^{-2}$	TO	$2{\cdot}3\times10^{-1}$	×
$2{\cdot}3\times10^{-1}$	TO	2·3	⊙
2·3	TO	23	+
23	TO	230	●

THESE SHOULD BE COMPARED WITH THE IDEAL FLUID THEORY, FIRST UNCORRECTED FOR THE EFFECT OF THE CONVERGING CHANNEL – – – – AND THEN WITH THIS CORRECTION INCLUDED. ———

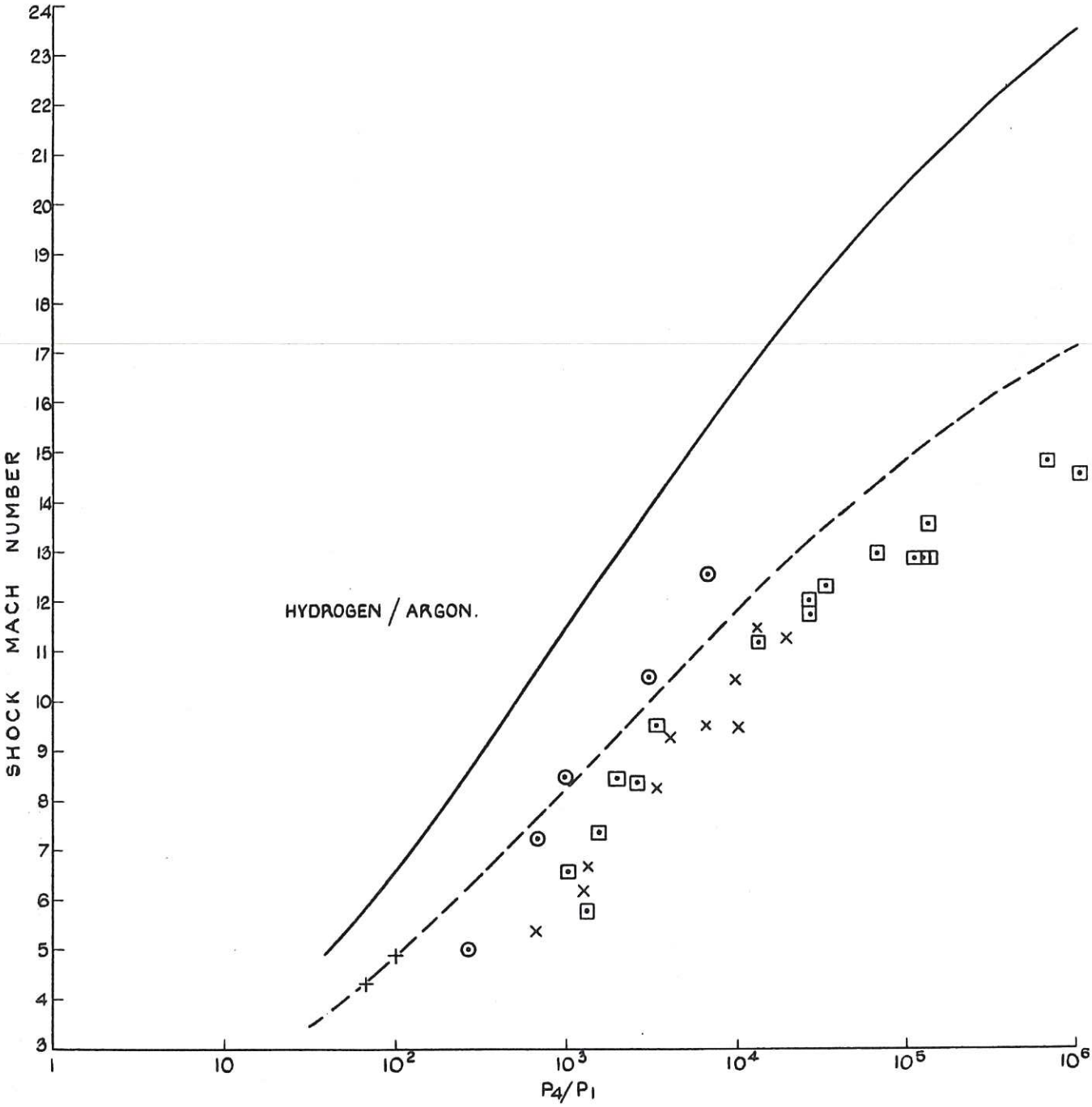

CLM-R18 .FIG. 5·3. SHOCK MACH NUMBER VERSUS P_4 / P_1 FOR HYDROGEN TO ARGON GAS COMBINATION.

THE POINTS REPRESENT EXPERIMENTAL DETERMINATIONS UNDER THE FOLLOWING CONDITIONS:-

PRESSURE RANGE (torr)			SYMBOL
$2{\cdot}3 \times 10^{-3}$	TO	$2{\cdot}3 \times 10^{-2}$	⊡
$2{\cdot}3 \times 10^{-2}$	TO	$2{\cdot}3 \times 10^{-1}$	×
$2{\cdot}3 \times 10^{-1}$	TO	2·3	⊙
2·3	TO	23	+

THESE SHOULD BE COMPARED WITH THE IDEAL FLUID THEORY, FIRST UNCORRECTED FOR THE EFFECT OF THE CONVERGING CHANNEL —— AND THEN WITH THIS CORRECTION INCLUDED. ————

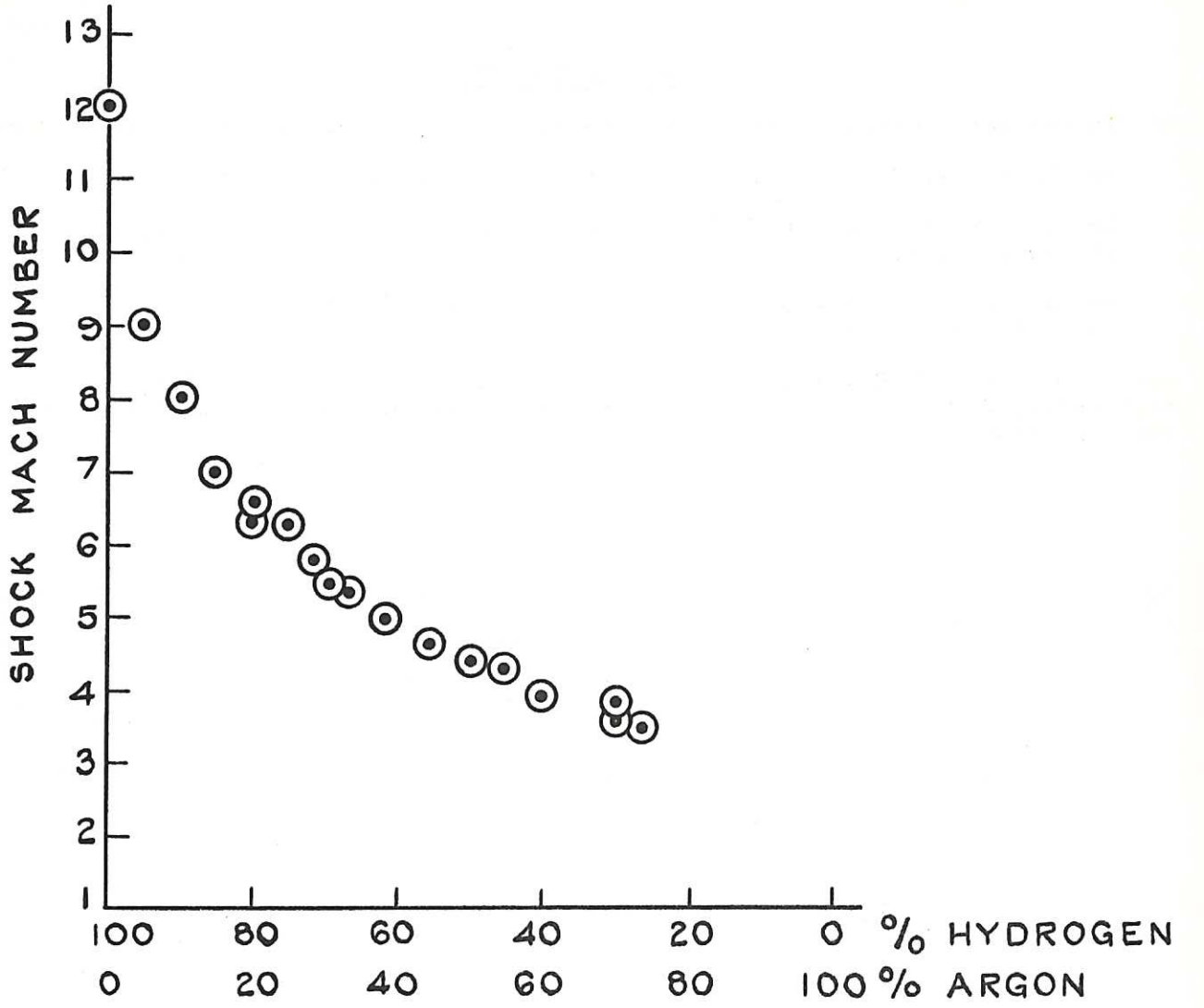

CLM-R18 FIG.5.4. SHOCK MACH NUMBER AS A FUNCTION OF THE RELATIVE PARTIAL PRESSURES OF HYDROGEN AND ARGON IN THE COMPRESSION CHAMBER.

CONSTANT TOTAL PRESSURE P_4 = 258.5 (torr)
EXPANSION CHAMBER GAS : ARGON AT P_1 = 0.0076mm OF MERCURY.
DIAPHRAGM : 0.001" MELINEX.

ACKNOWLEDGEMENTS

94. We are particularly indebted to the following members of Culham Laboratory:

Mr. W. Millar for advice and assistance with electronics design.

Dr. J.R. Storey and Dr. K.T. Dolder who have assisted by reading parts of the manuscript.

Mr. S.G.F. Blewett who assisted at all stages of the assembly and calibration of the shock tube.

and also to Mr. R. Bateman and Mr. D.A. Dunkason of the Design Office, Engineering Division, A.E.R.E., who assisted with the engineering design of the apparatus.

APPENDIX

Theory of a Gold Film Thermal Transducer

Temperature Rise of the Film

95. Suppose that initially the film and plastic backing material are at a temperature T_1 and the film is then suddenly placed in contact, at time $t = 0$, with a gas at a higher temperature T_2. This situation is realised in the shock tube except that there is fluid flow as well as heat flow present. The gold film is 5×10^{-5}mm thick so the effect of the film on the heat flow may be neglected. Then the temperature everywhere, at all times $t > 0$, will be determined solely by the backing material and the gas.

96. If all heat flow is normal to the film surface then temperature changes occur initially at the interface and spread gradually into the two media. Because the film is so thin it will take up a uniform temperature - the interface temperature T. We wish to find expressions for T as a function of T_2, T_1, the time and the thermal properties of the two media.

97. An estimate is also needed of the effect of the finite thickness of the gold film on its response time. The problem may be illustrated thus:-

Medium 2 (Gas)	Medium 1 (Plastic Backing Material)
$t < 0$ temperature T_2	T_1
$t \geq 0$ temperature $T_2 + V_2(x,t)$	$T_1 + V_1(x,t)$
Thermal conductivity K_2	K_1
Density ρ_2	ρ_1
Specific Heat c_2	c_1
Thermal diffusivity $k_2 = K_2/\rho_2 c_2$	$k_1 = K_1/\rho_1 c_1$

O ——————————→ x

98. The two media 1 and 2, initally separate, come in contact at time $t = 0$. In either medium the equation governing the conduction of heat, assuming k_2 and k_1 are constant is:

$$\delta^2 V/\delta x^2 = (\tfrac{1}{k})\delta V/\delta t \qquad 1$$

which has to be solved with the following boundary conditions:-

$$V_2(x,t) = V_1(x,t) \text{ for } t < 0, \qquad 2$$

$$V_2(0,t) + T_2 = V_1(0,t) + T_1 \text{ for } t > 0, \qquad 3$$

$$\left.\begin{aligned} V_2(x,t) &\longrightarrow 0 \text{ as } x \longrightarrow -\infty \\ V_1(x,t) &\longrightarrow 0 \text{ as } x \longrightarrow +\infty \end{aligned}\right\} \qquad 4$$

$$K_2(\delta V_2/\delta x)_{x=0} = K_1(\delta V_1/\delta x)_{x=0} \text{ for } t > 0 \qquad 5$$

Equation 5 expresses the continuity of heat flow across the interface. The The solution of equation is treated fully, by Carslaw and Jaeger[22] and is:-

$$V_1(x,t) = T' \text{ erfc } (\tfrac{1}{2}.\ x\ (k_1 t)^{-\frac{1}{2}}), \qquad 6$$

$$V_2(x,t) = -(T_2 - T_1 - T') \text{ erfc } (-\tfrac{1}{2}\ x\ .(k_2 t)^{-\frac{1}{2}} \qquad 7$$

where $T' = (T_2 - T_1)/(1 + (\rho_1 K_1 c_1/\rho_2 K_2 c_2)^{\frac{1}{2}}$ 8

in particular $V_1\ (0,t) = T'$, 9

which means that the interface temperature T = T' and jumps instantaneously on contact and then remains constant with time.

Effect of Finite Heat Capacity of the Film

99. In the above treatment we have neglected the thermal capacity of the gold film. If we take this into account but still neglect the diffusion time across the thickness of the film (as we may do for thin films of high thermal conductivity) then it can be shown by similar methods that equation 9 becomes:

$$V_1(0,t) = T'(1 - \exp\ (t/t_o)\ \text{erfc}\ (t/t_o)^{\frac{1}{2}}) \qquad 10$$

where $t_o = C^2/K_1\rho_1 c_1$ 11

and C = thermal capacity of the film per unit area = $\rho_t c_t x_t$. ρ_t, c_t, x_t being the density, specific heat and thickness of the film. Note that t_o increases as the square of the film thickness. The table below shows the growth of $V_1(0,t)$ with time, computed from equation 10. The third row shows actual values of t for a typical value of t_o. For a gold film 200 atoms thick x_t is 5×10^{-5} mm and t_o is 2×10^{-8} secs.

$V_1(0,t)/T^1$	t/t_o	t in microseconds. for $t_o = 2 \times 10^{-8}$ seconds
0.00	0.00	0.00
0.39	0.25	0.005
0.57	1.00	0.02
0.68	2.25	0.04
0.74	4.00	0.08
0.79	6.25	0.12
0.84	12.00	0.28
0.89	25.00	0.50
0.94	100.00	2.00
0.97	400.00	8.00
0.99	2,500.00	5.00

Expected Signal Sensitivity Limit

100. In this section the expected temperature rise of the film is calculated and from this the amplitude of the voltage pulse for a given shock in air. For this gas at a pressure p_1 = 760 mercury and a temperature 293°K.

$$K_2 = 5.7 \times 10^{-5} \text{ cal/deg/C/cm/cm}^2\text{/sec.}$$
$$\rho_2 = 1.3 \times 10^{-3} \cdot (\rho_2/\rho_1)^{\frac{1}{2}} \text{ gm/cc.}$$
$$c_2 = 1.7 \times 10^{-1} \text{ cal/gm/deg. C.}$$

101. The plastic backing material is 5×10^{-2} mm thick and its thermal constants are:

$$K_1 = 1.0 \times 10^{-3} \text{ cal/deg C/cm/cm}^2\text{/sec.}$$
$$\rho_1 = 2.0 \text{ gms/cc.}$$
$$c_1 = 2.0 \times 10^{-1} \text{ cal/gm/deg. C.}$$

Inserting these values in equation 8 and rearranging

$$T^1 = (T_2 - T_1) \left[(\rho_2 K_2 c_2)/(\rho_1 k_1 c_1)\right]^{\frac{1}{2}} \qquad 12$$
$$T^1 = (T_2 - T_1) \ (\rho_2/\rho_1)^{\frac{1}{2}} \times 5.8 \times 10^{-3} \qquad 13$$

where $(\rho_2/\rho_1)^{\frac{1}{2}}$ is the density ratio across the shock front and varies with increasing shock strength from 1 to 4 for a monatomic gas and 1 to 6 for a diatomic gas.

102. If the film has a resistance R of 55 ohms, carries a current I of 10 mA and has a temperature coefficient α of resistance[5][23] of 1.55×10^{-3} then if room temperature is 293 °K the signal voltage V is given by

$$V = I\alpha R \, T^1 \qquad 14$$
$$V = (T_2/T_1 - 1)(\rho_2/\rho_1)^{\frac{1}{2}} \times 1.45 \times 10^{-3} \text{ volts} \qquad 15$$

This signal V is effectively in series with film. Values of the ratio T_2/T_1 as a function of shock Mach number M are tabulated by Lukasiewicz[10]; these values have been inserted in equation 15 to obtain the theoretical curve of Figure 4.9 for an initial pressure p_1 = 760 mm of mercury. For other values of p_1 it follows from equation 8 that V varies as $(p_1)^{\frac{1}{2}}$.

Limitations of the Theory

103. The effect of the gas flow behind the shock on the rate of heat transfer has so far been neglected. According to Rott and Hartimian[24] the temperature T^1 (equation 8) should be multiplied by a quantity which depends on Mach number M and ranges from unity for weak shocks to about 1.5 for strong shocks. No account has been taken of the various relaxation processes following the shock, when the temperature may exceed its final value and K_2, ρ_2 and c_2 are not necessarily constant. A discussion of the temperature dependence of K for nitrogen under conditions when ionization has to be taken into account is given by King[25].

REFERENCES

(1) Hide, R., 1955; The experimental shock wave programme at Harwell. A.E.R.E. P 17/P5.

(2) Dolder, K. and Hide, R., 1958; An experiment on the interaction between a strong shock and a magnetic field. Nature, 181, 1116-1118.

(3) Dolder, K. and Hide, R., 1960; Experiments on the passage of a shock wave through a magnetic field. Reviews of Modern Physics, 32, 770-779.

(4) Dolder, K. and Hide, R., 1957; Bibliography on shock waves, shock tubes and allied topics; A.E.R.E. GP/R 2055.

(5) Price, N.H., 1957; Gold film thermometers and their application to the shock tube. A.E.R.E. GP/R 2442.

(6) Hide, R. and Millar, W., 1956; A preliminary investigation of shocks in a curved channel. A.E.R.E. GP/R 1918.

(7) Thonemann, P.C. and others, 1958; Production of high temperatures and nuclear reactions in a gas discharge. Nature, 181, 217-220.

(8) Holder, D.W. and North, R.J. Optical methods for examining the flow in high speed wind tunnels. NPL/AERO/300.

(9) Bitondo, D. and Lobb, R.K., 1950; Design and construction of a shock tube. Institute of Aerophysics, University of Toronto, Report No.3.

(10) Lukasiewicz, J., 1952; Shock tube theory and applications. National Aeronautical Establishment, Canada, Report 15.

(11) Lobb, R.K., 1950; A study of supersonic flows in a shock tube. Institute of Aerophysics, University of Toronto, Report 8.

(12) Glass, I.I., 1958; Theory and performance of simple shock tubes. Institute of Aerophysics, University of Toronto, Review No.12, Part 1.

(13) Hide, R., 1956; Note on converging shocks. A.E.R.E. GP/M 191.

(14) Hide, R., 1956; Note on the production of strong shocks. A.E.R.E. GP/M 202.

(15) Hide, R., 1957; Shock heating of a wriggling discharge. A.E.R.E. GP/R 2328.

(16) Chester, W., 1954; Phil. Mag. Ser.7, 45, 1293.

(17) Whitham, G.B., 1957; A new approach to problems of shock dynamics. Part 1; Two-dimensional problems. J. Fluid Mech., 2, 145-171.

(18) Blackman, V.H., 1956; Vibrational relaxation in O_2 and N_2. J. Fluid Mech., 1, 61-85.

(19) Lewis, I. and Wells, F., 1954; Millimicrosecond Pulse Techniques. Pergamon Press.

(20) Owen, P.R., 1954; The Manchester University Shock Tube. Aeronautical Research Council, Report ARC-17238.

(21) Goodfellow, H., 1954; Single and repetitive light sources. A.W.R.E. Report Number 0-11/53.

(22) Carslaw, H.S. and Jaeger, J.C., 1947; Operational Methods in Applied Mathematics. 2nd edition, Oxford U.P.

(23) Ennos, A.E., 1957; Highly conducting films prepared by vacuum evaporation. Brit. J. App. Phys., 8, 113-117.

REFERENCES

(continued)

(24) Rott, N. and Hartuniam, R., 1955; On the heat transfer to the walls of a shock tube. Cornell University Report OSR-TN-55-442.

(25) King, L.A., 1954; The positive column of high and low current arcs. Nature, 174, p.1008.

List of abbreviations used in references:

A.E.R.E. - Atomic Energy Research Establishment,
United Kingdom Atomic Energy Authority,
Harwell, Berkshire, England.

A.W.R.E. - Atomic Weapons Research Establishment,
United Kingdom Atomic Energy Authority,
Aldermaston, Berkshire, England.

N.P.L. - National Physical Laboratory,
Teddington,
Middlesex, England.

Available from
HER MAJESTY'S STATIONERY OFFICE
York House, Kingsway, London W.C. 2
423 Oxford Street, London W. 1
13a Castle Street, Edinburgh 2
109 St. Mary Street, Cardiff
39 King Street, Manchester 2
50 Fairfax Street, Bristol 1
2 Edmund Street, Birmingham 3
80 Chichester Street, Belfast
or through any bookseller.

Printed in England

S. O. Code No. 91 - 3 - 12 -51